torcentrum vid Universitet i Linköping) for generous grants of computer time on the Cray X-MP/416 supercomputer. Grants from the Swedish Natural Science Research Council to S.G. are gratefully acknowledged.

**Registry No.** Benzene, 71-43-2; nitronium, 14522-82-8; methyl nitrate (protonated), 99573-80-5; toluene, 108-88-3.

**Supplementary Material Available:** Tables giving internal coordinate systems (in Z-matrix form) and optimized geometrical parameters (36 pages). Ordering information is given on any current masthead page.

# The Puckering Inversion Barrier and Vibrational Spectrum of Cyclopentene. A Scaled Quantum Mechanical Force Field Algorithm

**Wesley D. Allen,*,† Attila G. Császár,‡ and David A. Horner§**

*Contribution from the Department of Chemistry, Stanford University, Stanford, California 94305, Failure Analysis Associates, Inc., 149 Commonwealth Drive, Menlo Park, California 94025, and Departments of Chemistry and Physics, North Central College, Naperville, Illinois 60566.*
*Received February 3, 1992*

**Abstract:** High-level ab initio quantum chemical studies have been performed to ascertain the equilibrium molecular structure and ring-puckering inversion barrier of cyclopentene, as well as the complete infrared and Raman spectra of cyclopentene-$d_0$, -*1*-$d_1$, -*1,2,3,3*-$d_4$, and -$d_8$. The planar ($C_{2v}$) and puckered ($C_s$) structures of cyclopentene have been optimized at the DZ(d) SCF and MP2 levels, and reasonable agreement with available experimental data is found. The DZ(d) MP2 prediction for the puckering angle is 23.4°, which compares favorably with several experimental values in the range 22–26°. High-level electron correlation treatments with extended basis sets are found to be necessary to converge the predicted puckering inversion barrier. In accord with experimental values, a final theoretical proposal of 235 ± 20 cm$^{-1}$ is derived for the vibrationless inversion barrier from a combination of TZ(d,p) MP4 and PZ(3d2f,2p1d) MP2 results. The fundamental vibrational frequencies (including intensity and polarization data) of cyclopentene isotopomers have been obtained from DZ(d) SCF force constants by using the scaled quantum mechanical (SQM) force field procedure. An improved SQM algorithm has been formulated which allows facile optimization of empirical scale factors to determine optimal quadratic force fields. Numerous reassignments are proposed among the 128 observed fundamental frequencies of the four isotopomers considered. It is shown that zero-point vibrational effects engender a substantial contribution to the empirically derived puckering inversion barrier.

## Introduction

As discussed in a 1979 review by Carreira, Lord, and Malloy,[1] many of the fundamental issues pertaining to low-frequency vibrations in small ring compounds are encountered in the investigation of representative molecules such as cyclobutane, cyclopentene, trimethylene oxide, 1,4-dioxadiene, tetrahydrofuran, and 1,4-dioxene. In this sense the cyclopentene molecule constitutes a prototype of large-amplitude, ring-puckering motion in the gas phase. In general, the low-frequency vibrational spectra of such molecules can be interpreted satisfactorily via one- and two-dimensional quantum mechanical models for ring puckering and/or twisting; however, coupling with the zero-point vibrational motions of the high-frequency normal modes must be considered in the analysis. In many cases the low-frequency spectroscopic information obtainable in the far-infrared region is incomplete, and the ring-puckering vibrations must be characterized from resulting difference bands associated with reference fundamentals in the mid-infrared region. Therefore, to fully resolve questions pertaining to the puckering dynamics of a small ring compound such as cyclopentene, not only are reliable results required for the equilibrium configuration and the ring puckering potential function but also a definitive analysis of the complete vibrational spectrum is needed.

Due to its prototypical characteristics, cyclopentene has become one of the most thoroughly studied examples of pseudo-four-membered-ring molecules with a double-minimum potential function for low-frequency puckering vibrations.[1-4] Over the course of the last few decades, the far-infrared,[9,14,15,20] mid-infrared,[5-8,12,13,16-21] Raman,[10-15,18-22] and microwave[23-25] spectra

† Stanford University.
‡ Stanford University; Failure Analysis Associates, Inc.
§ North Central College.

(1) Carreira, L. A.; Lord, R. C.; Malloy, T. B. *Top. Curr. Chem.* **1979**, *82*, 1.
(2) Laane, J. *Pure Appl. Chem.* **1987**, *59*, 1307.
(3) Harthcock, M. A.; Laane, J. *J. Mol. Spectrosc.* **1982**, *91*, 300.
(4) Malloy, T. B., Jr.; Bauman, L. E.; Carreira, L. A. *Top. Stereochem.* **1979**, *11*, 97.
(5) Beckett, C. W.; Freeman, N. K.; Pitzer, K. S. *J. Am. Chem. Soc.* **1948**, *70*, 4227.
(6) Sverdlov, L. M.; Krainov, E. N. *Opt. Spectrosc. (USSR)* **1959**, *6*, 214.
(7) LeRoy, A.; Thonvenout, J. C. *C. R. Acad. Sci.* **1967**, *B37*, 545.
(8) Ueda, T.; Shimanouchi, T. *J. Chem. Phys.* **1967**, *47*, 5018.
(9) Laane, J.; Lord, R. C. *J. Chem. Phys.* **1967**, *47*, 4941.
(10) Durig, J. R.; Carreira, L. A. *J. Chem. Phys.* **1972**, *56*, 4966.
(11) Chao, T. H.; Laane, J. *Chem. Phys. Lett.* **1972**, *14*, 595.
(12) Wertz, D. W.; Bocian, D. F.; Hazouri, M. J. *Spectrochim. Acta* **1973**, *29A*, 1439.
(13) Harris, W. C.; Longshore, C. T. *J. Mol. Struct.* **1973**, *16*, 187.
(14) Villarreal, J. R.; Bauman, L. E.; Laane, J.; Harris, W. C.; Bush, S. F. *J. Chem. Phys.* **1975**, *63*, 3727.
(15) Villarreal, J. R.; Bauman, L. E.; Laane, J. *J. Phys. Chem.* **1976**, *80*, 1172.
(16) Villarreal, J. R.; Laane, J.; Bush, S. F.; Harris, W. C. *Spectrochim. Acta* **1979**, *35A*, 331.
(17) Green, W. H. *J. Chem. Phys.* **1970**, *52*, 2156.
(18) Besnard, M.; Lassegues, J.-C.; Guissani, Y.; Leicknam, J.-L. *Mol. Phys.* **1984**, *53*, 1145.
(19) Villarreal, J. R. Ph.D. Thesis, Department of Chemistry, Texas A&M University, 1976.
(20) Lascombe, J.; Cavagnat, D.; Lassegues, J. C.; Rafilipomanana, C.; Biran, C. *J. Mol. Struct.* **1984**, *113*, 179.
(21) Rafilipomanana, C.; Cavagnat, D.; Lassegues, J. C. *J. Mol. Struct.* **1985**, *129*, 215.
(22) Rafilipomanana, C.; Cavagnat, D.; Cavagnat, R.; Lassegues, J. C.; Birat, C. *J. Mol. Struct.* **1985**, *127*, 283.

0002-7863/92/1514-6834$03.00/0 

of cyclopentene have been studied extensively, while at the same time several mathematical analyses[26-34] have been performed to address the large-amplitude puckering motion from a theoretical point of view. The first published attempt to obtain the molecular structure of cyclopentene from its microwave spectrum was that of Rathjens[23] in 1962, in which numerous structural assumptions were used in conjunction with the three observed rotational constants to extract a value of 22.3° for the dihedral puckering angle. Rathjens[23] also reported results from a one-dimensional vibrational analysis by Chan which gave a barrier height to puckering inversion of about 230 $cm^{-1}$. A reinvestigation of the microwave spectrum by Butcher and Costain[24] in 1965 yielded a separation of 0.91 $cm^{-1}$ for the lowest puckering inversion doublet, from which an estimate of 250–400 $cm^{-1}$ was obtained for the barrier to planarity. In 1967 Ueda and Shimanouchi[8] observed a series of ring-puckering difference bands in the region (2600–2900 $cm^{-1}$) of the $\nu_5$, $\alpha$-$CH_2$ symmetric stretching fundamental and then fit a one-dimensional potential function to the data to find a puckering angle of 22.1° and a barrier height of 244.6 $cm^{-1}$. A concurrent analysis by Laane and Lord[9] produced similar values of 23.3° and 232 $cm^{-1}$, respectively, from direct observations of ring-puckering transitions in the 18–300-$cm^{-1}$ region. Subsequently, Scharpen[25] showed that a barrier height of 232 ± 5 $cm^{-1}$ is indeed consistent with the available microwave data. A gas-phase electron diffraction (GED) analysis of the molecular structure of cyclopentene was performed by Davis and Muecke[36] in 1970. Several assumptions concerning the positions of the hydrogen atoms and the magnitudes of vibrational amplitudes were made in the refinement, but a reasonably reliable structure for the carbon framework was established, a puckering angle of 28.8 (25)° being found in particular.

The body of ring-puckering data for cyclopentene burgeoned after 1970. Extensive and detailed work by Laane and co-workers[11,14-16,28] afforded one-dimensional potential functions for cyclopentene-$d_0$, -*1*-$d_1$, -*1,2,3,3*-$d_4$, and -$d_8$ with corresponding puckering inversion barriers of 233, 231, 224, and 215 $cm^{-1}$, respectively. The observed isotopic dependence of the inversion barrier was later resolved[28] by invoking a two-dimensional dynamical model in which ring-puckering and ring-twisting motions were coupled. A simultaneous fit to the voluminous far-infrared data for the four isotopomers yielded a two-dimensional potential surface with an inversion barrier of 232 $cm^{-1}$ and an optimal dihedral puckering angle of 26°. Numerous other studies[20-22,26,27,29] prior to 1985 of the ring-puckering dynamics in cyclopentene provided results consistent with the two-dimensional surface of Laane et al.[30] In 1986 Hamilton, Light, and Whaley[31] addressed the ring-puckering issue using an inverse perturbation analysis with local correction functions, concluding that "the actual barrier height is higher by about 6 $cm^{-1}$ than the 232 $cm^{-1}$ of Laane's potential." More recently, by using periodic functions in a one-dimensional model Hamiltonian, Sztraka[34] determined a puckering angle of 27.7° and a barrier height of 232.4 $cm^{-1}$ for cyclopentene-$d_0$. Finally, in 1991 Champion et al.[32] performed a semirigid bender analysis of the experimental ring-puckering data with the aid of ab initio geometrical structures, this study resulting in values of 230 ± 2 $cm^{-1}$ for the barrier height and 25.4 ± 1° for the puckering angle.[35]

Experimental studies focusing on the vibrational spectrum of cyclopentene above 400 $cm^{-1}$ are much less numerous than those concerned with ring puckering in the far-infrared region. In 1973 Harris and Longshore[13] recorded and assigned the infrared and Raman spectra of cyclopentene-$d_0$ from 300 to 3200 $cm^{-1}$. However, the 1979 study of Villarreal, Laane, Bush, and Harris[16] (hereafter referred to as VLBH) is the most extensive work to date in that detailed vibrational assignments and normal coordinate analyses were obtained for four isotopomers, cyclopentene-$d_0$, -*1*-$d_1$, -*1,2,3,3*-$d_4$, and -$d_8$, a total of 128 fundamentals being considered altogether. Nevertheless, some deficiencies in the empirically derived quadratic force field are present which can be resolved with the aid of ab initio data.

Only a limited number of theoretical studies on cyclopentene have been reported in the literature.[37-45] Rosas, Cooper, and Laane[37] have used molecular mechanics (MM2) methods to calculate the barriers to planarity and/or pseudorotation for a series of 23 small ring molecules, providing an important test of the reliability of these empirically-based techniques. A puckering angle of 30° and an inversion barrier of 252 $cm^{-1}$ were found for cyclopentene. However, by using an earlier parametrization of the molecular mechanics method, Allinger[38] obtained substantially different results, viz. 19° for the puckering angle and 143 $cm^{-1}$ for the barrier. Intermediate values for these quantities from molecular mechanics methods have also been reported.[45] Application of the CNDO/2 semiempirical method to obtain the equilibrium structure of cyclopentene results in an erroneous puckering angle of only 1°.[41] Among the ab initio studies of cyclopentene,[32,39-44] no high-level determinations of the ring-puckering potential function have been reported. Saebo, Cordell, and Boggs[44] obtained a DZ SCF puckering angle of 13.6° and an inversion barrier of 31 $cm^{-1}$, while Miller, Schulman, and Disch[39] report analogous 6-31G* SCF values of 14.1° and ca. 100 $cm^{-1}$, respectively. At the STO-3G SCF level, the puckering angle is only 10.3°,[39b] whereas the barrier at the 4-31G** SCF level is only 97 $cm^{-1}$.[32] Thus, Hartree–Fock theory appears to be inadequate in predicting the puckering angle and inversion barrier of cyclopentene regardless of the basis set employed. To our knowledge, no detailed ab initio studies of the vibrational spectrum of cyclopentene have appeared.

While the geometrical structure and puckering inversion barrier of cyclopentene appear to be well established experimentally, it is clear that substantial discrepancies with theory remain to be resolved for this important, prototypical molecule. Indeed, Laane and co-workers[37] state in their 1990 paper that "even the most sophisticated ab initio calculations fail at evaluating the barriers to planarity [of small ring molecules] with any degree of reliability". Therefore, the first goal of this paper is to respond to the cited challenge by performing a high-level ab initio investigation of the puckering inversion barrier of cyclopentene. Contained in the experimentally derived inversion barrier are zero-point vibrational contributions arising from the high-frequency normal modes of the molecule. Accurate vibrational analyses of both the puckered ($C_s$) and planar ($C_{2v}$) conformations of cyclopentene are necessary to determine these contributions. Moreover, as stated above, improvements in the empirical force field of VLBH are needed to provide a definitive analysis of the

(23) Rathjens, G. W., Jr. *J. Chem. Phys.* **1962**, *36*, 2401.
(24) Butcher, S. S.; Costain, C. C. *J. Mol. Spectrosc.* **1965**, *15*, 40.
(25) Scharpen, L. H. *J. Chem. Phys.* **1968**, *48*, 3552.
(26) Malloy, T. B., Jr. *J. Mol. Spectrosc.* **1972**, *44*, 504.
(27) Malloy, T. B., Jr.; Carreira, L. A. *J. Chem. Phys.* **1979**, *71*, 2488.
(28) Bauman, L. E.; Killough, P. M.; Cooke, J. M.; Villarreal, J. R.; Laane, J. *J. Phys. Chem.* **1982**, *86*, 2000.
(29) Smithson, T. L.; Duckett, J. A.; Paul, R.; Wieser, H.; Birss, F. W. *Mol. Phys.* **1984**, *53*, 1495.
(30) Laane, J. *J. Mol. Struct.* **1985**, *126*, 99.
(31) Hamilton, I. P.; Light, J. C.; Whaley, K. B. *J. Chem. Phys.* **1986**, *85*, 5151.
(32) Champion, R.; Godfrey, P. D.; Bettens, F. L. *J. Mol. Spectrosc.* **1991**, *147*, 488.
(33) Sztraka, L. *Acta Phys. Hung.* **1988**, *63*, 143.
(34) Sztraka, L. *J. Mol. Struct.* **1990**, *218*, 327.
(35) A compilation of experimentally determined barrier heights and ring puckering angles can be found in Table I of ref 32.
(36) Davis, M. I.; Muecke, T. W. *J. Phys. Chem.* **1970**, *74*, 1104.
(37) Rosas, R. L.; Cooper, C.; Laane, J. *J. Phys. Chem.* **1990**, *94*, 1830.
(38) Allinger, N. L.; Sprague, J. T. *J. Am. Chem. Soc.* **1972**, *94*, 5734.
(39) (a) Miller, M. A.; Schulman, J. M.; Disch, R. L. *J. Am. Chem. Soc.* **1988**, *110*, 7681. (b) Schulman, J. M.; Miller, M. A.; Disch, R. L. *J. Mol. Struct. THEOCHEM* **1988**, *169*, 563.
(40) Evanseck, J. D.; Mareda, J.; Houk, K. N. *J. Am. Chem. Soc.* **1990**, *112*, 73.
(41) De Alti, G.; Decleva, P. *J. Mol. Struct.* **1977**, *41*, 299.
(42) Wiberg, K. B.; Bonneville, G.; Dempsey, R. *Isr. J. Chem.* **1983**, *23*, 85.
(43) Leroy, G.; Mangen, J. M.; Sana, M.; Weiler, J. *J. Chim. Phys., Phys.-Chim. Biol.* **1977**, *74*, 351.
(44) Saebo, S.; Cordell, F. R.; Boggs, J. E. *J. Mol. Struct. THEOCHEM* **1983**, *104*, 221.
(45) Lenz, T. G.; Vaughan, J. D. *J. Phys. Chem.* **1989**, *93*, 85.

vibrational spectrum of cyclopentene. Thus, the second goal of this paper is to determine a force field which reproduces the observed fundamental frequencies of all isotopomers to approximately 1%, while simultaneously revealing any missing and erroneous assignments. Finally, in realizing this second goal, a concise review and an improved mathematical formulation of the scaled quantum mechanical (SQM) force field procedure[46] are advanced. This third goal is the subject of the next two sections, after which results pertaining to the first two objectives are presented.

## Review of SQM Methodology

An immense number of theoretical investigations[46-52] has shown that the self-consistent-field (SCF) level of theory not only is a very useful starting point for investigating infrared and Raman spectra of moderately-sized polyatomic molecules but also is frequently sufficient to provide definitive predictions. Due to basis set incompleteness, electron correlation effects, reference geometry errors, and mechanical anharmonicity, SCF harmonic vibrational frequencies for ordinary, valence-bonded molecules typically display a systematic 10–15% overestimation of experimental fundamental frequencies.[46-56] For triatomic and tetraatomic molecules, numerous examples[57-63] exist of much higher quality predictions (generally less than 2% error) of fundamental vibrational frequencies. Many of these results have been obtained using variational procedures to solve the vibrational problem and advanced electronic structure methods to provide the underlying potential energy surfaces, the latter methods including multireference configuration interaction (MRCI), coupled-cluster singles and doubles, including in cases a perturbative estimate for triple excitations [CCSD and CCSD(T)], and the coupled electron pair approximation (CEPA). However, the use of rigorous techniques to determine the vibrational dynamics of larger systems may not be possible, and the application of highly correlated methods to larger species is prohibitive in cost and may be unnecessary.[64]

To date the most widely used correlated methods for determining harmonic vibrational frequencies of moderately-sized polyatomics[65-70] are second-order Møller–Plesset perturbation theory (MP2) and single-reference configuration interaction singles and doubles theory (CISD), although CCSD techniques show much promise. Several efforts to append anharmonic corrections to correlated harmonic frequencies by employing recently developed analytic SCF third derivative procedures have been successful.[71-75] For example, in 1987 Lee, Allen, and Schaefer[73] used a triple-$\zeta$ + double polarization (TZ2P) basis set to compute two-reference CISD harmonic frequencies and SCF anharmonicities for ethylene. The deviations of the theoretical fundamentals from their experimental counterparts ranged from −1.9% to +3.3%, the average absolute error being only 2.6%. For additional discussion the reader is referred to a 1986 review by Hess, Schaad, Čársky, and Zahradnik[47] on theoretical calculations of vibrational spectra or to the systematic ab initio studies of vibrational anharmonicity by Allen and co-workers.[71,72]

In general, to obtain force fields which predict fundamental frequencies within 1% of experiment (as typically sought), some combination of empirical observations and ab initio calculations is currently necessary for all but the smallest polyatomic molecules. In early (1974) applications of this idea to ethane, ethylene, acetylene, and formaldehyde, Pulay and Meyer[76,77] accounted for systematic overestimations in SCF diagonal quadratic force constants by applying fixed scale factors of 0.90 and 0.80 for stretching and bending coordinates, respectively. The theoretical off-diagonal force constants were left unaltered in this approach. Shortly thereafter, Botschwina and co-workers,[78-80] among others,[81-83] implemented a technique of fitting diagonal force constants directly to experimental fundamentals while fixing the off-diagonal interaction constants to their ab initio values. In 1976 a more elaborate scaling scheme was introduced by Blom and Altona,[84] and several noteworthy applications soon followed.[85-87] Their technique involved the partitioning of coordinates which are similar chemically into various groups, e.g. CH stretches, CC stretches, or CCH bends. Each group was assigned a variable scale factor for the diagonal force constants, whereas all interaction constants were treated together with a single, additional scale factor. Determination of the scale factors was achieved via least-squares fitting to selected fundamental frequencies which were known well experimentally.

The scheme for combining empirical and ab initio data which has been most widely adopted and most fully developed is the scaled quantum mechanical (SQM) force field method of Pulay

(46) Pulay, P.; Fogarasi, G.; Pongor, G.; Boggs, J. E.; Vargha, A. *J. Am. Chem. Soc.* **1983**, *105*, 7037.
(47) Hess, B. A., Jr.; Schaad, L. J.; Čársky, P.; Zahradnik, R. *Chem. Rev.* **1986**, *86*, 709.
(48) Hehre, W. J.; Radom, L.; Schleyer, P. v. R.; Pople, J. A. *Ab Initio Molecular Orbital Theory*; Wiley-Interscience: New York, 1986.
(49) Pulay, P. *Mol. Phys.* **1969**, *17*, 197; **1970**, *18*, 473.
(50) Pulay, P. In *Modern Theoretical Chemistry*; Schaefer, H. F., III, Ed.; Plenum Press: New York, 1977; Vol. 4, pp 153–185.
(51) Pulay, P.; Fogarasi, G.; Pang, F.; Boggs, J. E. *J. Am. Chem. Soc.* **1979**, *101*, 2550.
(52) Fogarasi, G.; Pulay, P. In *Vibrational Spectra and Structure*; Durig, J. R., Ed.; Elsevier: Amsterdam, 1985; Vol. 14, pp 125–219.
(53) Pople, J. A.; Schlegel, H. B.; Krishnan, R.; DeFrees, D. J.; Binkley, J. S.; Frisch, M. J.; Whiteside, R. A.; Hout, R. F., Jr.; Hehre, W. J. *Int. J. Quantum Chem. Symp.* **1981**, *15*, 269.
(54) DeFrees, D. J.; McLean, A. D. *J. Chem. Phys.* **1985**, *82*, 333.
(55) (a) Yamaguchi, Y.; Schaefer, H. F., III *J. Chem. Phys.* **1980**, *73*, 2310. (b) Yamaguchi, Y.; Frisch, M. J.; Gaw, J. F.; Schaefer, H. F., III; Binkley, J. S. *J. Chem. Phys.* **1986**, *84*, 2262.
(56) Pupyshev, V. I.; Panchenko, Y. N.; Bock, C. W.; Pongor, G. *J. Chem. Phys.* **1991**, *94*, 1247.
(57) Sexton, G. J.; Handy, N. C. *Mol. Phys.* **1984**, *51*, 1321.
(58) McLean, A. D.; Bunker, P. R.; Escribano, R. M.; Jensen, P. *J. Chem. Phys.* **1987**, *87*, 2166.
(59) Petsalakis, I. D.; Theodorakopoulos, G.; Wright, J. S.; Hamilton, I. P. *J. Chem. Phys.* **1990**, *92*, 2440.
(60) Rendall, A. P.; Lee, T. J.; Taylor, P. R. *J. Chem. Phys.* **1990**, *92*, 7050.
(61) Botschwina, P.; Zilch, A.; Werner, H.-J.; Rosmus, P.; Reinsch, E.-A. *J. Chem. Phys.* **1986**, *85*, 5107.
(62) Weis, B.; Rosmus, P.; Yamashita, K.; Morokuma, K. *J. Chem. Phys.* **1990**, *92*, 6635.
(63) Harding, L. B.; Ermler, W. C. *J. Comput. Chem.* **1985**, *6*, 13.
(64) Császár, A. G.; Allen, W. D. Manuscript in preparation.
(65) (a) Simandiras, E. D.; Handy, N. C.; Amos, R. D. *Chem. Phys. Lett.* **1987**, *133*, 324. (b) Simandiras, E. D.; Amos, R. D.; Handy, N. C.; Lee, T. J.; Rice, J. E.; Remington, R. B.; Schaefer, H. F., III *J. Am. Chem. Soc.* **1988**, *110*, 1388.
(66) Handy, N. C.; Gaw, J. F.; Simandiras, E. D. *J. Chem. Soc., Faraday Trans. 2* **1987**, *83*, 1577.
(67) Binkley, J. S.; Frisch, M. J.; Schaefer, H. F., III *Chem. Phys. Lett.* **1986**, *126*, 1.
(68) Simandiras, E. D.; Handy, N. C.; Amos, R. D. *J. Phys. Chem.* **1988**, *92*, 1739.
(69) Hess, B. A., Jr.; Allen, W. D.; Michalska, D.; Schaad, L. J.; Schaefer, H. F., III *J. Am. Chem. Soc.* **1987**, *109*, 1615.
(70) Allen, W. D.; Bertie, J. E.; Falk, M. V.; Hess, B. A., Jr.; Mast, G. B.; Othen, D. A.; Schaad, L. J.; Schaefer, H. F., III *J. Chem. Phys.* **1986**, *84*, 4211.
(71) Clabo, D. A., Jr.; Allen, W. D.; Remington, R. B.; Yamaguchi, Y.; Schaefer, H. F., III *Chem. Phys.* **1988**, *123*, 187.
(72) Allen, W. D.; Yamaguchi, Y.; Császár, A. G.; Clabo, D. A., Jr.; Remington, R. B.; Schaefer, H. F., III *Chem. Phys.* **1990**, *145*, 427.
(73) Lee, T. J.; Allen, W. D.; Schaefer, H. F., III *J. Chem. Phys.* **1987**, *87*, 7062.
(74) Gaw, J. F.; Handy, N. C. *Chem. Phys. Lett.* **1985**, *121*, 321.
(75) Gaw, J. F.; Handy, N. C. In *Geometrical Derivatives of Energy Surfaces and Molecular Properties*; Jørgensen, P., Simons, J., Eds.; Reidel: Dordrecht, 1986; pp 79–94.
(76) Pulay, P.; Meyer, W. *Mol. Phys.* **1974**, *27*, 473.
(77) Meyer, W.; Pulay, P. *Theor. Chim. Acta* **1974**, *32*, 253.
(78) Botschwina, P. *Chem. Phys. Lett.* **1974**, *29*, 98.
(79) Bleicher, W.; Botschwina, P. *Mol. Phys.* **1975**, *30*, 1029.
(80) Botschwina, P.; Meyer, W.; Semkow, A. M. *Chem. Phys.* **1976**, *15*, 25.
(81) Fogarasi, G.; Pulay, P.; Molt, K.; Sawodny, W. *Mol. Phys.* **1977**, *33*, 1565.
(82) Christe, K. O.; Curtis, E. C.; Sawodny, W.; Härtner, H.; Fogarasi, G. *Spectrochim. Acta* **1981**, *37A*, 549.
(83) Pouchan, C.; Liotard, D.; Dargelos, A.; Chaillet, M. *J. Chim. Phys.* **1976**, *73*, 1046.
(84) Blom, C. E.; Altona, C. *Mol. Phys.* **1976**, *31*, 1377.
(85) Blom, C. E.; Altona, C. *Mol. Phys.* **1977**, *34*, 177.
(86) Blom, C. E.; Otto, L. P.; Altona, C. *Mol. Phys.* **1976**, *32*, 1137.
(87) (a) Blom, C. E.; Altona, C. *Mol. Phys.* **1977**, *33*, 875. (b) Blom, C. E.; Altona, C.; Oskam, A. *Mol. Phys.* **1977**, *34*, 557.

and co-workers.[46] As in the scheme of Blom and Altona, a scale factor for each group of chemically similar coordinates is assigned for the diagonal quadratic force constants. However, the interaction force constants are not scaled independently but according to the geometric mean of the scale factors for the respective diagonal elements, i.e.

$$F_{ij}(\mathrm{SQM}) = (\tau_i\tau_j)^{1/2}F_{ij}(\text{ab initio}) \qquad (1)$$

where $\tau_i$ and $\tau_j$ denote the scale factors for coordinates $i$ and $j$, respectively. The scale factors are either determined via a simultaneous least-squares fit to the fundamental frequencies of a parent compound and related isotopomers or congeners or fixed to standard values calibrated in previous SQM studies on related chemical systems. Because ab initio quadratic force constants are scaled in the SQM technique to reproduce experimental fundamental frequencies, the final scale factors account simultaneously for basis set, electron correlation, reference geometry, and anharmonicity effects. There is no rigorous justification for the use of eq 1 in scaling the off-diagonal force constants, but empirical and methodological experience with the technique has provided ample validation of this choice. In particular, if an appropriate set of internal coordinates is chosen, the largest off-diagonal force constants are usually reproduced by (unscaled) ab initio methods within 10–30%;[52] for example, the important stretch–stretch interaction terms are typically overestimated by this amount.[88] Thus, optimum scale factors[46,52,89] for the largest interaction constants tend to lie in the same range as those for the dominant diagonal terms, and the joint scaling in eq 1 is usually well based. Selection of a minimum number of scale factors is found to yield force fields compatible with experimental frequencies to within 20 $cm^{-1}$ in most cases, thus approaching the limit of accuracy achievable within the harmonic approximation. Two methodological advantages of the SQM technique over that of Blom and Altona are that (a) chemically dissimilar, off-diagonal couplings are not restricted to the same scale factor and (b) the results are invariant to linear transformations among coordinates within the same group.[46,52]

A uniform prescription for performing SQM analyses was proposed by Pulay and co-workers[46,52] after systematic studies of the method had been completed for several chemical systems. The prescription involves four facets: (1) the selection of a reference geometry obtained by adding standard, empirical corrections[51,84,90,91] to SCF optimum geometries; (2) the choice of a standard set of internal coordinates[51,92,104] to facilitate transferability of scale factors between molecules; (3) the use of a balanced and cost-effective basis set (e.g. 4-21G[51]) to determine quadratic force constants at the chosen reference geometry; and (4) the implementation of scale factors either calibrated for similar systems or reoptimized on the known experimental frequencies of the primary system of concern to provide the quadratic force field via eq 1. If standardized scale factors are used in part 4, then the SQM approach can be aptly described as a priori (but not ab initio) in that high-accuracy predictions of vibrational spectra can be made without empirical observations for the particular molecules of concern. One example of the success of a priori SQM techniques is in the prediction of the vibrational spectra of substituted benzenes.[89,93–98] In the representative case of pyridine,[93] after correction of a few of the experimental assignments, the mean deviation for the non-CH stretching frequencies was found to be 5.7 $cm^{-1}$. Other scaling methods have been proposed,[99–101] such as the use in eq 1 of the arithmetic mean[99,100] rather than the geometric mean of the scale factors, but none of these schemes has been widely adopted.

There is a plethora of published studies in which the SQM method or a variant of it has been applied to the prediction of vibrational spectra of molecules ranging in size from formaldehyde[46] to cubane[102] and naphthalene.[103] An extensive but incomplete list of SQM studies containing 165 entries is given in the supplementary material of this paper. In the investigation reported here, the basic concepts embodied in eq 1 are utilized to determine the best available force field for cyclopentene, but departures are made from the recommendations of Pulay and Fogarasi[46] in the choice of the reference geometry. Furthermore, in developing a new software package to perform SQM analyses, improvements in the central algorithms have been formulated, as described in the next section.

## Algorithm for the SQM Procedure

For isotopomer A, the vector $\mathbf{Q}^A$ of normal coordinates is related in first order to the vector $\mathbf{S}^A$ of internal displacement coordinates by[108,109]

$$\mathbf{S}^A = \mathbf{L}^A\mathbf{Q}^A \qquad (2)$$

where the familiar $\mathbf{L}^A$ matrix is given by

$$\mathbf{L}^A = (\mathbf{G}^A)^{1/2}\mathbf{C}^A \qquad (3)$$

In eq 3 $\mathbf{G}^A$ is the conventional G matrix for isotopomer A, and $\mathbf{C}^A$ contains the eigenvectors of the symmetric matrix $\mathbf{M}^A$:[109]

(88) In this regard the mention of several counterexamples is warranted. In the case of benzene[89] and substituted benzenes,[93–98] a significant overestimation of the CC/CC coupling constants is observed at the SCF level which must be corrected in the SQM scheme by introducing extra scale factors for the appropriate constants.[89] Similarly, for the allyl radical[105] the MR-ACPF CC/CC coupling constant is smaller than the MCSCF constant by about 25%. In contrast, inclusion of dynamical electron correlation causes an increase in the CC stretch couplings in butadiene and hexatriene.[106] It seems that dynamical correlation reduces the coupling of adjacent CC bonds of the same length and enhances the coupling for alternating CC bonds. The case of $CO_2$ should also be mentioned, where the CO/CO stretch coupling is predicted at the SCF level to be almost twice as large as the well-established experimental value. Even the corresponding CISD value is too large by about 40%. Note also that the curvature of potential functions for linear bends associated with triple bonds (as in HCN, $C_6H_5CN$, HCCH, and $C_6H_5CCH$) is also poorly predicted at the SCF level, as indicated by the corresponding optimum scale factors in the range 0.60–0.65.[97,98] A proper treatment of linear bending motion is an apparent challenge for theory, as even highly correlated wave functions with extended basis sets predict bending frequencies that are extremely sensitive to the particular level of theory used.[107]

(89) Pulay, P.; Fogarasi, G.; Boggs, J. E. *J. Chem. Phys.* **1981**, *74*, 3999.

(90) (a) Schäfer, L.; Van Alsenoy, C.; Scarsdale, J. N. *J. Mol. Struct.* **1982**, *86*, 349. (b) Geise, H. J.; Pyckhout, W. In *Stereochemical Applications of Gas-Phase Electron Diffraction*; Hargittai, I., Hargittai, M., Eds.; VCH Publishers: New York, 1988; Part A, pp 321–346.

(91) The most extensive list of corrections available involves the 4-21G SCF level of theory.[51,90] Pulay and co-workers[92] have recently proposed an alternative scheme, in which "offset forces", i.e. standard, predetermined forces, are applied along the corresponding bond-stretching coordinates throughout the geometry optimization, rather than simply correcting the bond lengths after the optimization.

(92) Pulay, P.; Fogarasi, G.; Zhou, X.; Taylor, P. W. *Vib. Spectrosc.* **1990**, *1*, 159.

(93) (a) Pongor, G.; Pulay, P.; Fogarasi, G.; Boggs, J. E. *J. Am. Chem. Soc.* **1984**, *106*, 2765. (b) Pongor, G.; Fogarasi, G.; Boggs, J. E.; Pulay, P. *J. Mol. Spectrosc.* **1985**, *114*, 445.

(94) Niu, Z.; Dunn, K. M.; Boggs, J. E. *Mol. Phys.* **1985**, *55*, 421.

(95) Xie, Y.; Boggs, J. E. *J. Comp. Chem.* **1986**, *7*, 158.

(96) Fogarasi, G.; Császár, A. G. *Spectrochim. Acta* **1988**, *44A*, 1067.

(97) Császár, A. G.; Fogarasi, G. *Spectrochim. Acta* **1989**, *45A*, 845.

(98) Császár, A. G.; Fogarasi, G.; Boggs, J. E. *J. Phys. Chem.* **1989**, *93*, 7644.

(99) Hipps, K. W.; Poshusta, R. D. *J. Phys. Chem.* **1982**, *86*, 4112.

(100) Avbelj, F.; Hodoscek, M.; Hadzi, D. *Spectrochim. Acta* **1985**, *41A*, 89.

(101) Ha, T.-K.; Meyer, R.; Günthard, H. H. *Chem. Phys. Lett.* **1978**, *59*, 17.

(102) Dunn, K. M.; Pulay, P.; Van Alsenoy, C.; Boggs, J. E. *J. Mol. Spectrosc.* **1984**, *103*, 268.

(103) Sellers, H.; Pulay, P.; Boggs, J. E. *J. Am. Chem. Soc.* **1985**, *107*, 6487.

(104) Duncan, J. L. *Spectrochim. Acta* **1964**, *20*, 1197.

(105) Szalay, P. G.; Császár, A. G.; Fogarasi, G.; Karpfen, A.; Lischka, H. *J. Chem. Phys.* **1990**, *93*, 1246.

(106) Szalay, P. G.; Karpfen, A.; Lischka, H. *J. Chem. Phys.* **1987**, *87*, 3530.

(107) Simandiras, E. D.; Rice, J. E.; Lee, T. J.; Amos, R. D.; Handy, N. C. *J. Chem. Phys.* **1988**, *88*, 3187.

(108) Wilson, E. B., Jr.; Decius, J. C.; Cross, P. C. *Molecular Vibrations*; Dover: New York, 1980.

(109) Califano, S. *Vibrational States*; Wiley & Sons: London, 1976; Chapter 4, pp 80–101.

$$\mathbf{M}^{\mathrm{A}}\mathbf{C}^{\mathrm{A}} \equiv (\mathbf{G}^{\mathrm{A}})^{1/2}\mathbf{F}(\mathbf{G}^{\mathrm{A}})^{1/2}\mathbf{C}^{\mathrm{A}} = \mathbf{C}^{\mathrm{A}}\mathbf{\Lambda}^{\mathrm{A}} \tag{4}$$

$\mathbf{F}$ denotes the quadratic force constant matrix of the molecule evaluated at the reference geometry, and $\mathbf{\Lambda}^{\mathrm{A}}$ is a diagonal matrix from which the harmonic vibrational frequencies $\omega_i^{\mathrm{A}}$ of the system are determined according to

$$\Lambda_{ij}^{\mathrm{A}} = \lambda_i^{\mathrm{A}}\delta_{ij} = \frac{\delta_{ij}}{\kappa}(\omega_i^{\mathrm{A}})^2 \tag{5}$$

where $\kappa$ is a conversion factor chosen to yield $\omega_i^{\mathrm{A}}$ in $\mathrm{cm}^{-1}$. In the standard SQM procedure, one obtains the force constant matrix $\mathbf{F}$ from the unscaled, ab initio force constant matrix $\mathbf{F}_0$ via

$$\mathbf{F} = \mathbf{T}^{1/2}\mathbf{F}_0\mathbf{T}^{1/2} \tag{6}$$

Equation 6 is simply the matrix formulation of eq 1 in which $\mathbf{T}$ is a diagonal matrix containing the scale factors $\tau_i$, i.e. $T_{ij} = \tau_i\delta_{ij}$. Because the internal coordinates are grouped into chemically similar sets, the number of unique scale factors $M$ is usually much smaller than the dimension of $\mathbf{T}$. For clarity, $\tau_i$, $\tau_j$, $\tau_m$, and $\tau_n$ are used here to denote simply the scale factor for the internal coordinate with the same index, whereas $\tau_a$, $\tau_b$, and $\tau_c$ are used to represent the unique scale factor of a chemically distinct set of coordinates.

The scale factors $\tau_a$ are selected to minimize the quantity

$$\Xi = \sum_{\mathrm{A}}\sum_{i} w_i^{\mathrm{A}}(\omega_i^{\mathrm{A}} - \nu_i^{\mathrm{A}})^2 \tag{7}$$

where the $\nu_i^{\mathrm{A}}$ values are the experimental fundamental frequencies (in $\mathrm{cm}^{-1}$), the $\omega_i^{\mathrm{A}}$ frequencies are those calculated from eqs 4 and 5, and the $w_i^{\mathrm{A}}$ factors are appropriately selected, fixed weights. The sum in eq 7 runs over all isotopomers A included in the least-squares fit and over all associated normal modes $i$. If experimental data are missing for a particular frequency, $w_i^{\mathrm{A}}$ is set to zero. Otherwise, selecting $w_i^{\mathrm{A}} \propto (\nu_i^{\mathrm{A}})^{-n}$, where $n = 0$, 1, or 2, is reasonable in the absence of prior knowledge concerning the precision of the experimental data. Pulay and co-workers[46,51] have recommended that $n = 1$ be utilized, but the choice is usually not critical.[52]

In our implementation of the SQM method, a full second-order Newton–Raphson algorithm[110] is employed to determine the scale factors which minimize $\Xi$. Denoting the estimate for the optimum set of scale factors at iteration $k$ as $\tau_k$, the update formula for the vector $\tau_{k+1}$ can be written as

$$\tau_{k+1} = \tau_k - \xi_k\mathrm{H}_k\mathbf{g}_k \tag{8}$$

where the gradient vector $\mathbf{g}_n$ and the inverse Hessian matrix $\mathbf{H}_n$ are defined by the equations

$$(\mathbf{g}_k)_a = \frac{\partial\Xi}{\partial\tau_a} \equiv (\Xi_k)^a \tag{9}$$

and

$$(\mathrm{H}_k^{-1})_{ab} = \frac{\partial^2\Xi}{\partial\tau_a\partial\tau_b} \equiv (\Xi_k)^{ab} \tag{10}$$

The scalar quantity $\xi_k$ may be chosen (especially in the early iterations) to explicitly minimize $\Xi$ along the direction vector $-\mathbf{H}_k\mathbf{g}_k$ via some interpolation scheme,[110] but merely setting $\xi_k = 1$ provides comparable convergence unless the initial guess for the scale factors is poor.

In order to invoke the optimization algorithm in eq 8, explicit formulas for $\Xi^a$ and $\Xi^{ab}$ are needed. From eq 7 one readily obtains

$$\Xi^a = 2\sum_{\mathrm{A}}\sum_{i} w_i^{\mathrm{A}}(\omega_i^{\mathrm{A}} - \nu_i^{\mathrm{A}})J_{ia}^{\mathrm{A}} = \kappa\sum_{\mathrm{A}}\sum_{i}\beta_i^{\mathrm{A}}D_{ii}^{\mathrm{A},a} \tag{11}$$

in which $\mathbf{J}^{\mathrm{A}}$ is the familiar Jacobian matrix defined by[109,111]

$$J_{ia}^{\mathrm{A}} \equiv \left(\frac{\partial\omega_i^{\mathrm{A}}}{\partial\tau_a}\right) \tag{12}$$

while

$$\beta_i^{\mathrm{A}} \equiv w_i^{\mathrm{A}}\left(1 - \frac{\nu_i^{\mathrm{A}}}{\omega_i^{\mathrm{A}}}\right) \tag{13}$$

and

$$D_{ii}^{\mathrm{A},a} \equiv \left(\frac{\partial\lambda_i^{\mathrm{A}}}{\partial\tau_a}\right) = \left(\frac{2}{\kappa}\right)\omega_i^{\mathrm{A}}J_{ia}^{\mathrm{A}} \tag{14}$$

By differentiating the $i = j$ elements of the expression (cf. eq 4)

$$\Lambda_{ij}^{\mathrm{A}} = \lambda_i^{\mathrm{A}}\delta_{ij} = [(\mathbf{C}^{\mathrm{A}})^{\mathrm{t}}\mathbf{M}^{\mathrm{A}}(\mathbf{C}^{\mathrm{A}})]_{ij} \tag{15}$$

and taking advantage of the orthonormality of the eigenvectors contained in $\mathbf{C}^{\mathrm{A}}$, one finds that the $D_{ii}^{\mathrm{A},a}$ values in eq 14 are merely the diagonal elements of the matrix

$$D_{ij}^{\mathrm{A},a} = \sum_{m}\sum_{n}(F_0)_{mn}\theta_{mn}^{a}L_{mi}^{\mathrm{A}}L_{nj}^{\mathrm{A}} \tag{16}$$

where

$$\theta_{mn} \equiv \sqrt{\tau_m\tau_n} \tag{17}$$

Note that $\theta_{mn}^{a}$ denotes a derivative of eq 17 with respect to $\tau_a$.

The expression for the second derivatives $\Xi^{ab}$ is somewhat tedious to derive but nevertheless can be simplified to the relatively compact form

$$\Xi^{ab} = \kappa\sum_{\mathrm{A}}\sum_{i}(\beta_i^{\mathrm{A}}D_{ii}^{\mathrm{A},ab} + \gamma_i^{\mathrm{A}}D_{ii}^{\mathrm{A},a}D_{ii}^{\mathrm{A},b}) + 2\kappa\sum_{\mathrm{A}}\sum_{i>j}^{*}\left(\frac{\beta_i^{\mathrm{A}} - \beta_j^{\mathrm{A}}}{\lambda_i^{\mathrm{A}} - \lambda_j^{\mathrm{A}}}\right)D_{ij}^{\mathrm{A},a}D_{ij}^{\mathrm{A},b} \tag{18}$$

in which

$$\gamma_i^{\mathrm{A}} \equiv \left(\frac{w_i^{\mathrm{A}}\nu_i^{\mathrm{A}}}{2\omega_i^{\mathrm{A}}\lambda_i^{\mathrm{A}}}\right) \tag{19}$$

and

$$D_{ij}^{\mathrm{A},ab} = \sum_{m}\sum_{n}(F_0)_{mn}\theta_{mn}^{ab}L_{mi}^{\mathrm{A}}L_{nj}^{\mathrm{A}} \tag{20}$$

In order to arrive at eq 18 from eq 11, one must differentiate the off-diagonal elements of eq 15 to obtain the derivatives of the $\mathbf{L}^{\mathrm{A}}$ matrix,[109] viz.

$$\left(\frac{\partial L_{mi}^{\mathrm{A}}}{\partial\tau_a}\right) = \sum_{k}L_{mk}^{\mathrm{A}}U_{ki}^{\mathrm{A},a} \tag{21}$$

where

$$U_{ki}^{\mathrm{A},a} = \frac{D_{ik}^{\mathrm{A},a}}{\lambda_i^{\mathrm{A}} - \lambda_k^{\mathrm{A}}} \tag{22}$$

for $k \neq i$, and $U_{ii}^{\mathrm{A},a} = 0$. The asterisk placed on the second summation in eq 18 indicates the exclusion of degenerate pairs of normal modes, for which $\lambda_i^{\mathrm{A}} = \lambda_j^{\mathrm{A}}$ and $w_i^{\mathrm{A}} = w_j^{\mathrm{A}}$.

To our knowledge, eq 18 has not been published previously. Current algorithms usually employ an approximate expression for the scale-factor Hessian matrix from linear least-squares theory:[109,111,112]

$$\Xi^{ab} \approx \sum_{\mathrm{A}}\sum_{i}J_{ia}^{\mathrm{A}}w_i^{\mathrm{A}}J_{ib}^{\mathrm{A}} \tag{23}$$

Equation 23 arises from eq 18 by completely neglecting the last summation, by setting the $\beta_i^{\mathrm{A}}$ values to zero, and by replacing the $\gamma_i^{\mathrm{A}}$ quantities with

(110) Walsh, G. R. *Methods of Optimization*; Wiley & Sons: London, 1975.

(111) Pongor, G.; Pulay, P. Program Description of SCALE2, a Computer Program for SQM Analyses.

(112) Shoemaker, D. P.; Garland, C. W.; Nibler, J. W. *Experiments in Physical Chemistry*, 5th ed.; McGraw-Hill: New York, 1989; pp 801–827.

$$(\gamma_i^A)' = \gamma_i^A\left(\frac{\omega_i^A}{\nu_i^A}\right) \tag{24}$$

Consequently, some deterioration in convergence is observed, especially in the later iterations of the algorithm.

Utilizing eqs 12, 14, 21, and 22, it is possible through extended manipulations to derive the somewhat unwieldy expression for the third derivatives of $\Xi$ with respect to the scale factors $\tau_a$, as reported in the supplementary material of this paper. This expression can be incorporated in the scale factor optimization algorithm through the application of a technique involving both macroiterations and microiterations: (1) in each macroiteration, $\Xi$ is expanded through third order by using the current $\tau_a$ values as a reference; (2) microiterations are performed according to eq 8 to yield the optimum $\tau_a$ values predicted by the third-order expansion, the gradient vector and Hessian matrices for each microiteration being derived from the $\Xi^a$, $\Xi^{ab}$, and $\Xi^{abc}$ values at the reference point; and (3) macroiterations and accompanying microiterations are repeated until convergence. This method is useful in cases where the initial guess for the scale factors is poor or in cases where multiple solutions for the scale factors appear in close proximity. Otherwise, the expense of generating the third derivatives is not justified because the second-order algorithm with the exact Hessian from eq 18 is so rapidly convergent that there is little opportunity for improvement.

The use of eq 18 for $\Xi^{ab}$ rather than eq 23 engenders improved formulas for the statistical quantities which characterize the least-squares fit. Let $\nu_i^{0,A}$ be the set of idealized experimental frequencies assumed to follow the harmonic approximation exactly, and let $\nu_i^A$ denote the observed experimental frequencies assumed to be normally distributed about the $\nu_i^{0,A}$ values. The scale factors which exactly reproduce the idealized $\nu_i^{0,A}$ data are symbolized as $\tau_a^0$, and $\hat{\tau}_a$ denotes the maximum likelihood estimate of $\tau_a^0$ obtained by minimization of $\Xi$. The use of the $\hat{\tau}_a$ values in eq 6 yields $\hat{\omega}_i^A$ values as estimators of $\nu_i^{0,A}$. The variance for the optimum scale factors is then predicted by

$$s^2(\tau_a) = \langle(\hat{\tau}_a - \tau_a^0)^2\rangle = 2\eta(\mathbf{H\Omega H})_{aa} \tag{25}$$

where the matrix $\mathbf{\Omega}$ is defined as

$$\mathbf{\Omega} \equiv 2\sum_A (\mathbf{J}^A)^t\mathbf{W}^A(\mathbf{J}^A) \tag{26}$$

and the factor $\eta$ is given by

$$\eta = \frac{\Xi_0}{N - 2\mathrm{tr}(\mathbf{H\Omega}) + \mathrm{tr}(\mathbf{H\Omega H\Omega})} \tag{27}$$

In eqs 25–27, $\mathbf{W}^A$ is a diagonal matrix containing the weighting factors, i.e. $W_{ij}^A = w_i^A\delta_{ij}$, $\Xi_0$ is the final (minimized) value of $\Xi$, $\mathbf{H}$ is the final inverse scale factor Hessian (see eqs 10 and 18), $N$ is the total number of experimental data points involved in the fit, and tr($\mathbf{A}$) denotes the trace of matrix $\mathbf{A}$. The corresponding values for the correlation coefficients $r_{ab}$ of the scale factors are obtained from

$$r_{ab} = \frac{\langle(\hat{\tau}_a - \tau_a^0)(\hat{\tau}_b - \tau_b^0)\rangle}{s(\tau_a)s(\tau_b)} = \frac{(\mathbf{H\Omega H})_{ab}}{\sqrt{(\mathbf{H\Omega H})_{aa}(\mathbf{H\Omega H})_{bb}}} \tag{28}$$

Finally, the standard errors in the predicted vibrational frequencies can be found from

$$s^2(\omega_i^A) = \langle(\hat{\omega}_i^A - \nu_i^{0,A})^2\rangle = 2\eta[(\mathbf{J}^A)(\mathbf{H\Omega H})(\mathbf{J}^A)^t]_{ii} \tag{29}$$

Equations 25, 27, 28, and 29 all reduce to conventional forms[111,112] if the approximation $\mathbf{H} \approx \mathbf{\Omega}^{-1}$ is made, whence tr($\mathbf{H\Omega}$) = $M$ = tr($\mathbf{H\Omega H\Omega}$), $M$ being the number of unique scale factors.

### Computational Details

Several basis sets were employed in this study: DZ, DZ(d), DZ(d,p), TZ(d,p), TZ(d,p)*, TZ(2d,p), TZ(2d1f,2p1d), QZ(d,p), QZ(2d,2p), and PZ(3d2f,2p1d). These basis sets range in number of contracted Gaussian functions (CGFs) from 66 in the DZ case to 393 in the PZ(3d2f,2p1d) set (vide infra Table IV). In the designation A($x$,$y$) used to denote these basis sets, A is descriptive of the sp basis for the molecular system, whereas $x$ and $y$ indicate the sets of polarization functions appended to the carbon and hydrogen atoms, respectively. A convenient and equitable means of describing the quality of the sp sets is afforded by the number of contracted p functions in the carbon basis; hence, A = DZ, TZ, or QZ in representing sets of double-$\zeta$ (2p) through quadruple-$\zeta$ (4p) quality. To avoid ambiguity, the largest basis set used here, involving C(5p) sets, is denoted as PZ, for "penta-$\zeta$".

The DZ basis is the C(9s5p/4s2p) and H(4s/2s) set of Huzinaga[113] and Dunning,[114,115] the hydrogen exponents being scaled by a factor of 1.2[2] as usual. Likewise, in the TZ and QZ cases, the carbon basis sets are Huzinaga–Dunning (10s6p/5s3p) and (10s6p/5s4p) contractions, respectively.[116,117] For hydrogen, the TZ and QZ sets are (5s/3s) and (6s/4s) contractions of the unscaled exponents of Huzinaga, as tabulated respectively by Dunning[117] and Allen and Schaefer.[118] In the PZ basis set, a C(13s8p/6s5p) contraction was constructed from the primitives of Partridge[119] according to (6,3,1,1,1,1) and (4,1,1,1,1) schemes for the s and p functions, respectively. The same H(6s/4s) set used for the QZ basis was also employed in the PZ case.

In the basis sets involving the DZ core, the polarization function exponents $\alpha_d$(C) = 0.80 and $\alpha_p$(H) = 0.75 were selected, which are optimal for Hartree–Fock wave functions. The same orbital exponents were employed in the basis denoted TZ(d,p)*, but in all other cases correlation-optimized polarization function exponents were utilized, as proposed by Dunning.[120] The exponents for the carbon 1d, 2d, and 3d sets are 0.550, (0.318, 1.097), and (0.228, 0.649, 1.848), respectively, whereas 0.761 and (0.485, 1.419) are the corresponding values for the 1f and 2f sets. In the case of hydrogen, the correlation-optimized exponents of the 1p, 2p, and 1d sets are, in order, 0.727, (0.388, 1.407), and 1.057. In all cases the d sets involved 6 Cartesian components, but the f sets included only the 7 true spherical harmonics.

Electronic wave functions were determined in this study by the single-configuration, self-consistent-field, restricted Hartree–Fock (SCF) method,[48,121] by the single-reference configuration interaction singles and doubles (CISD) method,[122–125] and by perturbative methods for the incorporation of electron correlation, including second-, third-, and fourth-order Møller–Plesset theory, i.e. MP2, MP3, and MP4(SDTQ).[126–129] Extrapolation of the perturbation series to estimate the infinite-order energy (MP∞) was performed using a formula suggested by Pople and co-workers.[130,131] Generally the carbon 1s core orbitals were frozen in the MP$n$ correlation treatments, unless otherwise indicated by the designation MP$n$(full). In the CISD wave functions, all of which involved the DZ(d) basis, both the carbon 1s core orbitals and the corresponding 1s* virtual orbitals were excluded from the active space. The DZ(d) CISD wave functions for the planar and puckered conformations of cyclopentene thus included 131 413 and 255 181 configuration state functions (CSFs), respectively.

The geometrical structures of the planar ($C_{2v}$) and puckered ($C_s$) forms of cyclopentene were optimized at the DZ(d) SCF and DZ(d) MP2(full) levels of theory using analytic gradient techniques. The residual Cartesian gradients were in all cases less than $10^{-7}$ hartree/bohr. The Cartesian quadratic force constants of the $C_{2v}$ and $C_s$ structures, as

(113) Huzinaga, S. *J. Chem. Phys.* **1965**, *42*, 1293.
(114) Dunning, T. H. *J. Chem. Phys.* **1970**, *53*, 2823.
(115) Dunning, T. H.; Hay, P. J. In *Modern Theoretical Chemistry*; Schaefer, H. F., III, Ed.; Plenum: New York, 1977; Vol. 3, pp 1–27.
(116) Huzinaga, S. *Approximate Atomic Functions*; Department of Chemistry Report: University of Alberta, 1971; Vol. 2.
(117) Dunning, T. H. *J. Chem. Phys.* **1971**, *55*, 716.
(118) Allen, W. D.; Schaefer, H. F., III *J. Chem. Phys.* **1988**, *89*, 329.
(119) Partridge, H. *Near Hartree–Fock Quality Gaussian Type Orbital Basis Sets for the First- and Third-Row Atoms*; NASA Technical Memorandum 101044.
(120) Dunning, T. H. *J. Chem. Phys.* **1989**, *90*, 1007.
(121) Roothaan, C. C. J. *Rev. Mod. Phys.* **1951**, *23*, 69.
(122) Shavitt, I. In *Modern Theoretical Chemistry*; Schaefer, H. F., III, Ed.; Plenum: New York, 1977; Vol. 3, pp 189–275.
(123) Brooks, B. R.; Schaefer, H. F., III *J. Chem. Phys.* **1979**, *70*, 5391.
(124) Saxe, P.; Fox, D. J.; Schaefer, H. F., III; Handy, N. C. *J. Chem. Phys.* **1982**, *77*, 5584.
(125) Langhoff, S. R.; Davidson, E. R. *Int. J. Quantum Chem.* **1974**, *8*, 61.
(126) Møller, C.; Plesset, M. S. *Phys. Rev.* **1934**, *46*, 618.
(127) Pople, J. A.; Binkley, J. S.; Seeger, R. *Int. J. Quantum Chem. Symp.* **1976**, *10*, 1.
(128) Krishnan, R.; Pople, J. A. *Int. J. Quantum Chem.* **1978**, *14*, 91.
(129) Krishnan, R.; Frisch, M. J.; Pople, J. A. *J. Chem. Phys.* **1980**, *72*, 4244.
(130) Pople, J. A.; Frisch, M. J.; Luke, B. T.; Binkley, J. S. *Int. J. Quantum Chem. Symp.* **1983**, *17*, 307.
(131) Handy, N. C.; Knowles, P. J.; Somasundram, K. *Theor. Chim. Acta* **1985**, *68*, 87.

well as the analogous dipole-moment and polarizability derivatives, were determined analytically[132-137] at the DZ(d) SCF level using the respective DZ(d) SCF optimized reference geometries. In the investigation of the ring-puckering barrier via high-level, single-point energy calculations, the DZ(d) MP2(full) optimum geometries were employed, unless stated otherwise. All electronic structure computations were performed with the program packages PSI[138] and GAUSSIAN90.[139]

All normal coordinate analyses, including IR and Raman intensity determinations, were performed in conjunction with the SQM procedure as implemented in the program INTDER.[140] The normal modes were characterized in internal coordinates by the total energy distribution (TED) method advocated by Pulay and Török.[141] The final IR intensities were computed in the double-harmonic approximation[142,143] by projecting the DZ(d) SCF Cartesian dipole-moment derivatives onto the corresponding normal-mode eigenvectors arising from the *scaled* quadratic force constants. In a similar fashion, the DZ(d) SCF polarizability derivatives were used in the prediction of Raman scattering activities ($R_i$) and depolarization ratios ($\rho_i$) from well-known formulas[135,144] involving derivatives of the trace and anisotropy of the polarizability tensor with respect to the normal coordinates $Q_i$. While the quantitative prediction of infrared and Raman intensities usually requires much larger basis sets than DZ(d) and perhaps some inclusion of electron correlation,[135] the qualitative utility of moderate-basis SCF intensity predictions in assigning experimental spectra is well documented.[48,52]

The SQM analysis involved several sequential steps (1–6) as outlined below. (1) DZ(d) SCF reference geometries were selected for the computation of the unscaled, ab initio force constants to avert ambiguities arising from the presence of nonzero forces.[50,64] (2) An appropriate set of internal coordinates was constructed,[51] as listed in Table I. Chemically similar coordinates were partitioned into one of ten sets to which variable scale factors were ascribed, as detailed in Table II. (3) Correspondences between unscaled ab initio frequencies and experimental band origins were established for the $d_0$ and $d_8$ isotopomers, by taking into account not only the expected 8–13% errors in the SCF frequencies but also previous experimental assignments,[16,19] IR and Raman intensity data, predicted and observed depolarization ratios, isotopic substitution data, and the correlation of experimental band shapes to the symmetry species of the ab initio normal modes. Initial values for the optimum scale factors were estimated from those correspondences which were unequivocal. (4) The initial scale factors were employed in a normal coordinate analysis to make preliminary assignments of the spectra of the $d_1$ and $d_4$ species. In this way a total of 66 conclusive assignments were found for the four isotopomers in which the scaled ab initio results matched those of VLBH.[16,19] (5) A first refinement of the scale factors was performed via a least-squares fit to the 66 frequencies identified above. The fundamental frequencies and normal modes, IR and Raman intensities, and depolarization ratios calculated using the refined scale factors were then compared with experimental data to make additional assignments. At this point only 20 of the 132 normal modes of the four cyclopentene isotopomers were left without experimental frequency assignments. (6) A second, final refinement of the scale factors was performed using the expanded list of 112 experimental fundamentals. The final normal coordinate analysis was then used to predict the positions of the remaining, unassigned bands. In all SQM fits, the weighting factors, $w_i^A$, in eq 7 were made proportional to $(\nu_i^A)^{-1}$.

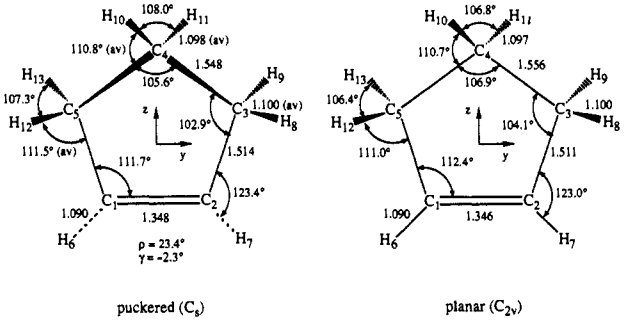


**Figure 1.** DZ(d) MP2(full) geometrical structures for cyclopentene. For the puckered conformation $\rho$ is the 1–5–3–4 dihedral puckering angle, and $\gamma$ is the out-of-plane bending angle for the vinyl hydrogens.

In Table II the optimized values of the scale factors are listed along with statistical data for the SQM fit, the error analysis being performed with the improved formulas (eq 25–29) reported above. The scale factors lie in the expected range,[46,52] viz. from 0.74 to 0.89, and the standard errors are remarkably small, less than 0.02 in all cases. The correlation coefficients ($r_{ab}$) reveal small covariances among the variable scale factors; the value of −0.44 for the correlation between the $CH_2$ wags and the CC stretches is the largest by far. Because the overestimation of quadratic force constants by Hartree–Fock theory typically increases with increasing bond order, it is not surprising that the scale factor for the C=C stretch is substantially smaller than those for the C—C and C—H stretches. Note that three of the four types of $CH_2$ bends are assigned to a single scale factor of 0.7960, whereas the $CH_2$ wags correspond to a separate factor of 0.7548. This choice is based on data from preliminary SQM refinements, which revealed that separate scale factors for the twists, rocks, and scissors are unnecessary but that inclusion of the $CH_2$ wags into this group significantly deteriorates the fit. Because the ring puckering mode is highly anharmonic, the scale factor for $S_{14}$ must be considered phenomenological in nature.

## Ring-Puckering Inversion Barrier

Geometric structural parameters for the planar ($C_{2v}$) and puckered ($C_s$) forms of cyclopentene are listed in Table III and depicted in Figure 1. In order to compare the DZ(d) SCF and MP2(full) results with the electron diffraction data of Davis and Muecke,[36] several constraints imposed during the GED refinement procedure should be highlighted: the equivalency of all C—H bond lengths; the coplanarity of the substituent atoms about the C=C bond; the coincidence of the bisectors of the HCH and adjacent CCC angles; and the perpendicularity of corresponding HCH and CCC planes. The present theoretical results show that these assumptions hold rather well. For example, in the $C_s$ structure the vinyl hydrogens are bent out of plane in the opposite direction of the puckering of the ring, but only by ca. 2° (see Figure 1); moreover, the C–H bond lengths cluster within a 0.011-Å range, variations which cannot be detected in GED analyses. The difference between the two C–C single bond lengths is observed experimentally to be 0.025 Å (with an uncertainty of about the same magnitude), which is comparable to the DZ(d) SCF and MP2 values of 0.033 and 0.034 Å, respectively. The agreement between the GED and DZ(d) MP2 carbon–carbon bond lengths is particularly good, the largest difference being 0.007 Å.

The most important structural parameter, the puckering angle $\rho$, was measured to be 28.8 (25)°, a value somewhat higher than the DZ(d) SCF and MP2 values of 20.4° and 23.4°, respectively. However, this angle is likely to be sensitive to the structural constraints employed in the GED refinement. Thus, we regard the most recent empirically-based proposal[32] of $\rho = 25.4 \pm 1°$ to be more reliable, consistent with the optimum puckering angle (26°) in the two-dimensional potential surface of Laane and co-workers.[28] In this case the DZ(d) MP2 value for $\rho$ would be

(132) Gaw, J. F.; Handy, N. C. *Annu. Rept. Progr. Chem. C* **1984**, *81*, 291.
(133) Pople, J. A.; Krishnan, R.; Schlegel, H. B.; Binkley, J. S. *Int. J. Quantum Chem. Symp.* **1979**, *13*, 225.
(134) Osamura, Y.; Yamaguchi, Y.; Saxe, P.; Vincent, M. A.; Gaw, J. F.; Schaefer, H. F., III *Chem. Phys.* **1982**, *72*, 131.
(135) Amos, R. D. In *Ab Initio Methods in Quantum Chemistry*; Lawley, K. P., Ed.; Wiley: New York, 1987; Vol. I, pp 99–153.
(136) Yamaguchi, Y.; Frisch, M. J.; Gaw, J. F.; Schaefer, H. F., III *J. Chem. Phys.* **1986**, *84*, 2262.
(137) Frisch, M. J.; Yamaguchi, Y.; Gaw, J. F.; Schaefer, H. F., III; Binkley, J. S. *J. Chem. Phys.* **1986**, *84*, 531.
(138) PSI 1.0, 1989, PSITECH, Inc., Watkinsville, GA.
(139) Frisch, M. J.; Head-Gordon, M.; Trucks, G. W.; Foresman, J. B.; Schlegel, H. B.; Raghavachari, K.; Robb, M.; Binkley, J. S.; Gonzalez, C.; DeFrees, D. J.; Fox, D. J.; Whiteside, R. A.; Seeger, R.; Melius, C. F.; Baker, J.; Martin, R. L.; Kahn, L. R.; Stewart, J. J. P.; Topiol, S.; Pople, J. A. Gaussian 90, Revision J, Gaussian, Inc., Pittsburgh, PA, 1990.
(140) Allen, W. D. Program INTDER, Stanford University, Stanford, CA.
(141) (a) Pulay, P.; Török, F. *Acta Chim. Hung.* **1965**, *44*, 287. (b) Keresztury, G.; Jalsovszky, G. *J. Mol. Struct.* **1971**, *10*, 304.
(142) Overend, J. In *Infrared Spectroscopy and Molecular Structure*; Davies, M., Ed.; Elsevier: Amsterdam, 1963; pp 345–376.
(143) Zerbi, G. In *Vibrational Intensities in Infrared and Raman Spectroscopy*; Person, W. B., Zerbi, G., Eds.; Elsevier: Amsterdam, 1982.
(144) Long, D. A. *Raman Spectroscopy*; McGraw Hill: New York, 1977.
(145) Mills, I. M. *J. Phys. Chem.* **1984**, *88*, 532.
(146) Egawa, T.; Yamamoto, S.; Ueda, T.; Kuchitsu, K. *J. Mol. Spectrosc.* **1987**, *126*, 231.
(147) Stone, J. M. R.; Mills, I. M. *Mol. Phys.* **1970**, *18*, 631.
(148) Miller, F. A.; Capwell, R. J. *Spectrochim. Acta* **1971**, *27A*, 947.
(149) Egawa, T.; Fukuyama, T.; Yamamoto, S.; Takabayashi, F.; Kambara, H.; Ueda, T.; Kuchitsu, K. *J. Chem. Phys.* **1987**, *86*, 6018.

**Table I.** Definition of Internal Coordinate Set for Cyclopentene[a]

| coordinates | description | coordinates | description |
|---|---|---|---|
| | | $A_1(A')$ | |
| $S_1 = r(1,2)$ | C=C stretch | $S_7 = c^{-1/2}[\alpha(5,4,3) + a\alpha(4,5,1) + a\alpha(4,3,2) + b\alpha(5,1,2) + b\alpha(3,2,1)]$ | ring bending |
| $S_2 = 2^{-1/2}[r(1,5) + r(2,3)]$ | C—C stretch | $S_8 = 2^{-1/2}[\beta(2,1,6) + \beta(1,2,7)]$ | CH sym in-plane bend |
| $S_3 = 2^{-1/2}[r(5,4) + r(3,4)]$ | C—C stretch | $S_9 = 2^{-1}[\beta(5,4,11) + \beta(3,4,11) + \beta(5,4,10) + \beta(3,4,10)]$ | $\beta$-$CH_2$ scissor |
| $S_4 = 2^{-1/2}[t(6,1) + t(7,2)]$ | C—H sym stretch | $S_{10} = 8^{-1/2}[\beta(4,5,13) + \beta(4,3,9) + \beta(4,5,12) + \beta(4,3,8) + \beta(1,5,13) + \beta(2,3,9) + \beta(1,5,12) + \beta(2,3,8)]$ | $\alpha$-$CH_2$ scissor |
| $S_5 = 2^{-1/2}[t(11,4) + t(10,4)]$ | $\beta$-$CH_2$ sym stretch | | |
| $S_6 = 2^{-1}[t(13,5) + t(9,3) + t(12,5) + t(8,3)]$ | $\alpha$-$CH_2$ sym stretch | $S_{11} = 8^{-1/2}[\beta(4,5,13) + \beta(4,3,9) + \beta(4,5,12) + \beta(4,3,8) - \beta(1,5,13) - \beta(2,3,9) - \beta(1,5,12) - \beta(2,3,8)]$ | $\alpha$-$CH_2$ wag |
| | | $A_2(A'')$ | |
| $S_{19} = 2^{-1}[t(13,5) - t(9,3) - t(12,5) + t(8,3)]$ | $\alpha$-$CH_2$ asym stretch | $S_{22} = 8^{-1/2}[\beta(4,5,13) - \beta(4,3,9) - \beta(4,5,12) + \beta(4,3,8) - \beta(1,5,13) + \beta(2,3,9) + \beta(1,5,12) - \beta(2,3,8)]$ | $\alpha$-$CH_2$ twist |
| $S_{20} = c^{-1/2}[b\tau(1,5,4,3) + b\tau(2,3,4,5) + a\tau(2,1,5,4) + a\tau(1,2,3,4) + \tau(5,1,2,3)]$ | ring twisting | $S_{23} = 8^{-1/2}[\beta(4,5,13) - \beta(4,3,9) - \beta(4,5,12) + \beta(4,3,8) + \beta(1,5,13) - \beta(2,3,9) - \beta(1,5,12) + \beta(2,3,8)]$ | $\alpha$-$CH_2$ rock |
| $S_{21} = 2^{-1}[\beta(5,4,11) - \beta(3,4,11) - \beta(5,4,10) + \beta(3,4,10)]$ | $\beta$-$CH_2$ twist | $S_{24} = 2^{-1/2}[\gamma(6,1,2,5) - \gamma(7,2,3,1)]$ | CH out-of-plane bend |
| | | $B_1(A')$ | |
| $S_{12} = 2^{-1/2}[t(11,4) - t(10,4)]$ | $\beta$-$CH_2$ asym stretch | $S_{16} = 8^{-1/2}[\beta(4,5,13) + \beta(4,3,9) - \beta(4,5,12) - \beta(4,3,8) - \beta(1,5,13) - \beta(2,3,9) + \beta(1,5,12) + \beta(2,3,8)]$ | $\alpha$-$CH_2$ twist |
| $S_{13} = 2^{-1}[t(13,5) + t(9,3) - t(12,5) - t(8,3)]$ | $\alpha$-$CH_2$ asym stretch | | |
| $S_{14} = d^{-1/2}[(a-b)\tau(1,2,3,4) - (a-b)\tau(2,1,5,4) + (1-a)\tau(2,3,4,5) - (1-a)\tau(1,5,4,3)]$ | ring puckering | $S_{17} = 8^{-1/2}[\beta(4,5,13) + \beta(4,3,9) - \beta(4,5,12) - \beta(4,3,8) + \beta(1,5,13) + \beta(2,3,9) - \beta(1,5,12) - \beta(2,3,8)]$ | $\alpha$-$CH_2$ rock |
| $S_{15} = 2^{-1}[\beta(5,4,11) + \beta(3,4,11) - \beta(5,4,10) - \beta(3,4,10)]$ | $\beta$-$CH_2$ rock | $S_{18} = 2^{-1/2}[\gamma(6,1,2,5) + \gamma(7,2,3,1)]$ | CH out-of-plane bend |
| | | $B_2(A'')$ | |
| $S_{25} = 2^{-1/2}[r(1,5) - r(2,3)]$ | C—C stretch | $S_{30} = 2^{-1/2}[\beta(2,1,6) - \beta(1,2,7)]$ | CH asym in-plane bend |
| $S_{26} = 2^{-1/2}[r(5,4) - r(3,4)]$ | C—C stretch | $S_{31} = 2^{-1}[\beta(5,4,11) - \beta(3,4,11) + \beta(5,4,10) - \beta(3,4,10)]$ | $\beta$-$CH_2$ wag |
| $S_{27} = 2^{-1/2}[t(6,1) - t(7,2)]$ | C—H asym stretch | $S_{32} = 8^{-1/2}[\beta(4,5,13) - \beta(4,3,9) + \beta(4,5,12) - \beta(4,3,8) + \beta(1,5,13) - \beta(2,3,9) + \beta(1,5,12) - \beta(2,3,8)]$ | $\alpha$-$CH_2$ scissor |
| $S_{28} = 2^{-1}[t(13,5) - t(9,3) + t(12,5) - t(8,3)]$ | $\alpha$-$CH_2$ sym stretch | | |
| $S_{29} = d^{-1/2}[(a-b)\alpha(4,5,1) - (a-b)\alpha(4,3,2) + (1-a)\alpha(5,1,2) - (1-a)\alpha(3,2,1)]$ | ring shearing | $S_{33} = 8^{-1/2}[\beta(4,5,13) - \beta(4,3,9) + \beta(4,5,12) - \beta(4,3,8) - \beta(1,5,13) + \beta(2,3,9) - \beta(1,5,12) + \beta(2,3,8)]$ | $\alpha$-$CH_2$ wag |

[a] The following notation has been used: $r(i,j) = C_i$–$C_j$ bond distance; $t(i,j) = H_i$–$C_j$ bond distance; $\alpha(i,j,k) = C_i$–$C_j$–$C_k$ bond angle; $\beta(i,j,k) = C_i$–$C_j$–$H_k$ bond angle; $\tau(i,j,k,l) = C_i$–$C_j$–$C_k$–$C_l$ torsion angle; $\gamma(i,j,k,l) = H_i$–$C_j$ out of $C_j$–$C_k$–$C_l$ plane angle; $a = \cos 144° = -0.8090$ and $b = \cos 72° = 0.3090$; $c = [1 + 2a^2 + 2b^2]$ and $d = [2(a-b)^2 + 2(1-a)^2]$ are normalization factors. See Figure 1 for numbering of atoms.

**Table II.** Optimized Values ($\tau_a$) and Statistics of SQM Fit for Scale Factors of Cyclopentene[a]

| | | | | correlation coefficients ($r_{ab}$) for $b$ = | | | | | | | | | |
|---|---|---|---|---|---|---|---|---|---|---|---|---|---|
| $a$ | $\tau_a$ | description | connected coordinates[b] | $a$ | 1 | 2 | 3 | 4 | 5 | 6 | 7 | 8 | 9 |
| 1 | 0.8148 (16) | C—H stretch | $S_4$–$S_6$, $S_{12}$, $S_{13}$, $S_{19}$, $S_{27}$, $S_{28}$ | | | | | | | | | | |
| 2 | 0.8818 (78) | C—C stretch | $S_2$, $S_3$, $S_{25}$, $S_{26}$ | 2 | −0.0071 | | | | | | | | |
| 3 | 0.7738 (71) | C=C stretch | $S_1$ | 3 | −0.0293 | −0.1211 | | | | | | | |
| 4 | 0.8509 (148) | ring bend | $S_7$, $S_{29}$ | 4 | −0.0084 | −0.1276 | −0.0417 | | | | | | |
| 5 | 0.7960 (32) | $CH_2$ twist, rock, scissor | $S_9$, $S_{10}$, $S_{15}$–$S_{17}$, $S_{21}$–$S_{23}$, $S_{32}$ | 5 | 0.0018 | −0.0939 | 0.0207 | −0.2175 | | | | | |
| 6 | 0.7548 (68) | $CH_2$ wag | $S_{11}$, $S_{31}$, $S_{33}$ | 6 | 0.0018 | −0.4358 | 0.0681 | 0.0292 | −0.0287 | | | | |
| 7 | 0.8228 (92) | CH in-plane bend | $S_8$, $S_{30}$ | 7 | 0.0045 | −0.1665 | −0.1177 | −0.1442 | 0.0080 | −0.1557 | | | |
| 8 | 0.7914 (113) | CH out-of-plane bend | $S_{18}$, $S_{24}$ | 8 | 0.0023 | 0.0138 | 0.0186 | −0.2617 | −0.2015 | 0.0077 | 0.0041 | | |
| 9 | 0.7444 (199) | ring pucker | $S_{14}$ | 9 | −0.0028 | 0.0028 | −0.0012 | 0.0159 | −0.0474 | 0.0013 | −0.0007 | −0.0120 | |
| 10 | 0.8532 (131) | ring twist | $S_{20}$ | 10 | −0.0003 | 0.0093 | −0.0003 | −0.0119 | −0.0995 | 0.0012 | 0.0029 | 0.1407 | −0.0001 |

[a] The standard errors are included in parentheses after the optimized values of the scale factors. The diagonal elements of the correlation matrix are $r_{aa} = 1$ by definition. [b] Defined in Table I.

Table III. Geometrical Structures for Cyclopentene[a]

| coordinate | planar ($C_{2v}$) DZ(d) SCF | planar ($C_{2v}$) DZ(d) MP2 (full) | puckered ($C_s$) DZ(d) SCF | puckered ($C_s$) DZ(d) MP2 (full) | expt[b] |
|---|---|---|---|---|---|
| $r(1,2)$ | 1.3232 | 1.3464 | 1.3243 | 1.3483 | 1.341 |
| $r(1,5) = r(2,3)$ | 1.5109 | 1.5109 | 1.5133 | 1.5137 | 1.519 |
| $r(5,4) = r(3,4)$ | 1.5519 | 1.5557 | 1.5460 | 1.5479 | 1.544 |
| $t(6,1) = t(7,2)$ | 1.0765 | 1.0904 | 1.0763 | 1.0902 | (1.096) |
| $t(11,4)$ | 1.0835 | 1.0966 | 1.0840 | 1.0972 | (1.096) |
| $t(10,4)$ | 1.0835 | 1.0966 | 1.0845 | 1.0979 | (1.096) |
| $t(13,5) = t(9,3)$ | 1.0864 | 1.0996 | 1.0878 | 1.1013 | (1.096) |
| $t(12,5) = t(8,3)$ | 1.0864 | 1.0996 | 1.0856 | 1.0985 | (1.096) |
| $\alpha(5,4,3)$ | 106.75 | 106.93 | 105.72 | 105.55 | 104.0 |
| $\alpha(4,5,1) = \alpha(4,3,2)$ | 103.88 | 104.09 | 102.93 | 102.85 | 103.0 |
| $\alpha(5,1,2) = \alpha(3,2,1)$ | 112.74 | 112.44 | 112.14 | 111.65 | 111.2 |
| $\beta(2,1,6) = \beta(1,2,7)$ | 124.71 | 124.63 | 124.90 | 124.87 | 121.8 |
| $\beta(5,4,11) = \beta(3,4,11)$ | 110.83 | 110.68 | 112.57 | 112.42 | |
| $\beta(5,4,10) = \beta(3,4,10)$ | 110.83 | 110.68 | 109.29 | 109.19 | |
| $\beta(4,5,13) = \beta(4,3,9)$ | 112.03 | 111.93 | 111.95 | 111.62 | |
| $\beta(4,5,12) = \beta(4,3,8)$ | 112.03 | 111.93 | 112.24 | 112.16 | |
| $\beta(1,5,13) = \beta(2,3,9)$ | 111.23 | 111.01 | 110.34 | 110.25 | |
| $\beta(1,5,12) = \beta(2,3,8)$ | 111.23 | 111.01 | 112.68 | 112.73 | |
| $\tau(1,2,3,4) = -\tau(2,1,5,4)$ | 0.00 | 0.00 | 12.47 | 14.26 | |
| $\tau(2,3,4,5) = -\tau(1,5,4,3)$ | 0.00 | 0.00 | -19.34 | -22.23 | |
| $\rho = 180° + \tau(1,5,3,4)$ | 0.00 | 0.00 | 20.4 | 23.4 | 28.8 |
| $\gamma(6,1,2,5) = \gamma(7,2,3,1)$ | 0.00 | 0.00 | -1.65 | -2.30 | 0.0 |
| total energy | -194.00154 | -194.69622 | -194.00206 | -194.69703 | |

[a] Bond distances in Å, angles in deg, total energies in hartree. See footnote *a* of Table I for coordinate definitions. The dihedral puckering angle is denoted by $\rho$. [b] See column c of Table I of ref 36. For standard error estimates of the reported parameters see the original publication. As highlighted by parentheses, all C–H distances were constrained to be equivalent in the GED analysis.

in error by only 2°, an assertion supported by additional structural predictions at the TZ(d,p) MP2 level.[150] A state-of-the-art electron diffraction study is needed to resolve this issue by incorporating technological advances of the past 20 years as well as the spectral and structural data reported here.

Total energies of the planar and puckered forms of cyclopentene at various levels of theory are tabulated in the supplementary material (Table X). The difficulty of predicting the puckering inversion barrier first becomes apparent from the total energies obtained at the DZ(d) SCF optimum geometries. The corresponding DZ(d) SCF and CISD barrier heights are found to be only 112.2 and 125.1 $cm^{-1}$, respectively, and addition of the Davidson correction[125] to the CISD results actually shifts the barrier back to 116.3 $cm^{-1}$, i.e. very close to the SCF prediction. Furthermore, appending p functions to the hydrogen atoms yields a barrier of 106.9 $cm^{-1}$ at the DZ(d,p) SCF level. Ostensibly these results show that the barrier height is insensitive to both basis set and electron correlation. Because the DZ(d) basis is usually quite reliable in predicting geometrical structures and conformational energy differences, the discrepancy of over 100 $cm^{-1}$ with the experimental barrier (232 $cm^{-1}$) initially proved to be a nonplussing phenomenon.

More detailed studies of the puckering inversion barrier using DZ(d) MP2(full) reference geometries are summarized in Table IV. Note that the SCF and MP*n* energies obtained with the DZ basis at these reference structures erroneously place the planar conformation *below* the puckered form. With all other basis sets the predictions are qualitatively correct, but at the SCF level a quantitative underestimation of the barrier height is seen to persist even in the Hartree–Fock limit. In particular, expansion of the basis past TZ(2d,1p) does not alter the inversion barrier more than 3 $cm^{-1}$, and the anomalously small 94.5-$cm^{-1}$ result obtained with the PZ(3d2f,2p1d) basis, which consists of 393 CGFs, is surely near the HF limit for the chosen reference geometries. The

Table IV. Theoretical Data for the Ring-Puckering Inversion Barrier of Cyclopentene[a,b]

| | SCF | MP2 | MP3 | MP4 | MP∞ |
|---|---|---|---|---|---|
| DZ (66) | -11.6 | -80.5 | -111.9 | -111.5 | |
| DZ(d) (96) | 94.6 (112.1) | 159.9 [177.1] | 100.8 | 120.9 | 120.5 |
| DZ(d,p) (120) | 88.4 | 147.7 | 74.6 | 96.3 | |
| TZ(d,p)* (148) | 118.7 | 319.8 | | | |
| TZ(d,p) (148) | 113.2 | 310.8 [309.5] | 213.8 | 252.6 | 253.0 |
| QZ(d,p) (171) | 115.9 | 317.1 [321.5] | | | |
| TZ(2d,1p) (178) | 95.5 | 262.7 | 171.8 | | |
| QZ(2d,2p) (225) | 92.6 | 285.4 | | | |
| TZ(2d1f,2p1d) (285) | 95.3 | 292.8 | | | |
| PZ(3d2f,2p1d) (393) | 94.5 | 275.4 | | | |

final proposal for bare barrier height: 235 ± 20 $cm^{-1}$

[a] The values reported, all in $cm^{-1}$, were obtained from single-point energy calculations performed for the planar ($C_{2v}$) and puckered ($C_s$) forms of cyclopentene at the respective DZ(d) MP2(full) geometries. For each basis set the total number of contracted Gaussian functions (CGFs) is listed in parentheses. [b] The inversion barriers listed in parentheses were obtained at the respective optimum geometries. The values reported in square brackets refer to calculations in which no orbitals were frozen.

first direct indication of the substantial contribution due to electron correlation is seen in the DZ(d) MP2 result of 159.9 $cm^{-1}$, but as the higher-order correlation contributions are included with this basis, an oscillation in the predictions occurs and convergence appears to be reached at a value of only 120 $cm^{-1}$. Therefore, even at the DZ(d) MP4(SDTQ) level of theory, the inversion barrier is only half as large as the experimental value. As indicated by the DZ(d,p) MP2–MP4 entries in Table IV, this discrepancy is not resolved by the inclusion of p functions on the hydrogen atoms.

The inadequacy of the DZ(d) and DZ(d,p) MP2-MP4 levels of theory in predicting the puckering inversion barrier is rooted in the deficiency of the double-$\zeta$ sp basis for the carbon atoms. Indeed, the TZ(d,p)* MP2 barrier (319.8 $cm^{-1}$) is twice as large as the analogous DZ(d) and DZ(d,p) values! The use of correlation-optimized exponents via the TZ(d,p) basis does not change the TZ(d,p)* MP2 result significantly, nor does the additional sp flexibility contained in the QZ(d,p) basis. These observations notwithstanding, the TZ(d,p) and QZ(d,p) MP2 predictions are not fully converged values. The second set of carbon d functions

(150) A reoptimization of the $C_{2v}$ and $C_s$ structures at the TZ(d,p) MP2 level resulted in a puckering angle of 26.8° and an inversion barrier of 330 $cm^{-1}$. Thus, a 3.4° increase in the puckering angle from the DZ(d) MP2 reference geometry is accompanied by a 19-$cm^{-1}$ increase in the barrier height. Both of these shifts should represent upper bounds on the variations at even higher levels of theory because the TZ(d,p) MP2 method significantly overestimates the inversion barrier. See Table XIII of the supplementary material for a tabulation of the TZ(d,p) MP2 structural parameters.

gives rise to a TZ(2d,1p) MP2 barrier of 262.7 $cm^{-1}$, whereas further addition of a set of carbon f functions and hydrogen p and d orbitals yields a TZ(2d1f,2p1d) MP2 prediction of 292.8 $cm^{-1}$. As gauged by the final PZ(3d2f,2p1d) energies, the MP2 basis set limit for the puckering inversion barrier appears to be 275 ± 15 $cm^{-1}$.

A final proposal for the barrier height can be derived from the prediction at the TZ(d,p) MP4 level of theory, which is the most computationally intensive procedure listed in Table IV. The computed barrier heights in the TZ(d,p) perturbation series are observed to oscillate as before, but the MP∞ extrapolation estimate of 253 $cm^{-1}$ is essentially the same as the directly determined MP4 value. In comparing analogous results in the DZ(d) and TZ(d,p) MP*n* series, it appears that basis set effects on the inversion barrier are very similar at the MP2 and MP4 levels; specifically, the MP4 shift in going from DZ(d) to TZ(d,p) is about 90% of the MP2 value. Further evidence for the similarity of basis set effects across the MP*n* series is gained by comparing the differences in the TZ(2d,1p) and TZ(d,p) inversion barriers at the MP2 and MP3 levels. The MP2 shift is −48 $cm^{-1}$, whereas the MP3 result is −42 $cm^{-1}$. Therefore, a correction due to basis set incompleteness of roughly −30 $cm^{-1}$ is suggested for the TZ(d,p) MP4 barrier as a consequence of the TZ(d,p) and PZ(3d2f,2p1d) MP2 determinations. Further relaxation of the $C_s$ and $C_{2v}$ reference geometries at higher levels of theory should increase the barrier by 10–20 $cm^{-1}$, insofar as higher inversion barriers are associated with larger puckering angles and $\rho$ is expected to increase by no more than 3°.[150] Finally, the correction due to the frozen-core approximation appears to be negligible. The DZ(d) MP2(full) barrier is 17 $cm^{-1}$ higher than its frozen-core counterpart, but this increase is reduced to less than 4 $cm^{-1}$ if the more flexible TZ(d,p) and QZ(d,p) basis sets are employed. It seems that the more complete the one-particle basis becomes, the less the effect of unfreezing the core in the *n*-particle space. In summary, consideration of the effects of basis set incompleteness, geometry relaxation, and frozen-core restrictions on the TZ(d,p) MP4 result engenders a final proposal of 235 ± 20 $cm^{-1}$ for the bare puckering inversion barrier height in cyclopentene.

While the final theoretical proposal for the inversion barrier appears to be in near perfect agreement with experiment; a direct comparison of these results is somewhat specious. The basic assumption behind experimental determinations of ring-puckering inversion barriers by spectroscopic methods[1,2] is that the large-amplitude motions can be separated from the other vibrational modes by a sudden/adiabatic approximation. It is known that this separation may not always be valid.[145,146] For example, in the case of cyclobutane, Kuchitsu and co-workers[146] demonstrated that while a one-dimensional potential gives a ring-puckering barrier of about 510 $cm^{-1}$,[147-149] a more elaborate two-dimensional model accounting for the coupling between the ring-puckering and $CH_2$-rocking motions yields a significantly lower barrier of 449 (9) $cm^{-1}$.

As described in the Introduction, several one- and two-dimensional models have been constructed empirically for cyclopentene, and in contrast to cyclobutane[146] the resulting puckering inversion barriers are very similar, the range being 230–240 $cm^{-1}$ with most published values lying near 232 $cm^{-1}$. Nevertheless, our SQM data reveal that the coupling with zero-point vibrational motions of higher frequency modes produces a significant contribution to the effective barrier height for ring puckering. Of the 32 vibrational modes which complement the ring-puckering motion in cyclopentene-$d_0$, the frequencies of nine change more than 10 $cm^{-1}$ in going from the puckered to planar conformations. The largest shifts of +93.2, −46.3, and −40.3 $cm^{-1}$ occur, in order, for $\nu_{17}$, $\nu_{16}$, and $\nu_{15}$ (see Table V below). Despite substantial cancellations among the frequency shifts, nonnegligible $C_s \rightarrow C_{2v}$ changes of +25.4, +24.7, +21.0, and +16.0 $cm^{-1}$ occur for the total zero-point vibrational energies of the complementary modes of cyclopentene-$d_0$, -*1*-$d_1$, -*1,2,3,3*-$d_4$, and -$d_8$, respectively. For these four isotopomers Laane and co-workers[14-16,28] report vibrationally-adiabatic barrier heights of 233, 231, 224, and 215 $cm^{-1}$ for the effective one-dimensional puckering potentials. After applying the ZPVE corrections listed above, values of 208, 206, 203, and 199 $cm^{-1}$ are found for the respective bare puckering inversion barriers. Note that the range of isotopic dependence in the empirically-derived barrier heights is cut in half merely by including changes in the zero-point vibrational energies of the complementary modes. In contrast, Laane et al.[28] have accounted for this isotopic dependence by using a two-dimensional model of ring puckering and twisting with no consideration of ZPVE in complementary modes. As stated several times above, the barrier height in the resulting two-dimensional potential is 232 $cm^{-1}$, and thus the shifts upon inclusion of ring twisting in the determination of the puckering inversion barrier are −1, +1, +8, and +17 $cm^{-1}$ respectively for the $d_0$, $d_1$, $d_4$, and $d_8$ isotopomers. Such shifts are at variance with the differences in the zero-point energies of the twisting modes in the planar and puckered forms, these differences lying uniformly in the range +6 to +8 $cm^{-1}$ according to the SQM data. These results highlight the importance of high-quality analyses of the vibrational spectra of isotopomers used in determinations of experimental barrier heights.

In summary, zero-point vibrational effects lead to minor inconsistencies in the empirical determination of the puckering inversion barrier of cyclopentene. The SQM vibrational analysis reported here suggests that the bare inversion barrier may be 20–30 $cm^{-1}$ smaller than the 232-$cm^{-1}$ barrier present in the two-dimensional potential surface of Laane and co-workers.[28] In any event the agreement between experiment and our final theoretical proposal of 235 ± 20 $cm^{-1}$ must be considered satisfactory.

**Vibrational Spectrum**

In Tables V–VIII complete vibrational assignments and final SQM frequency, intensity, and depolarization data are presented for cyclopentene-$d_0$, -*1*-$d_1$, -*1,2,3,3*-$d_4$, and -$d_8$. Only the experimental band origins judged to be the most reliable are listed therein; a complete tabulation of available experimental data is given elsewhere.[16,19] At the DZ(d) SCF reference geometry which was used in the SQM analysis, cyclopentene is puckered by 20.4°, so the $d_0$ and $d_8$ isotopomers possess a $\sigma(xz)$ plane of symmetry and belong to the $C_s$ point group, while the $d_1$ and $d_4$ species have no symmetry (see Figure 1). However, because the carbon framework is not far removed from planarity, most of the normal coordinates approach higher symmetry, either $C_{2v}$ or $C_s$, the additional plane of symmetry being $\sigma(yz)$ in both cases.[151] In fact, by performing the vibrational analyses with the symmetry-adapted $C_{2v}$ internal coordinates defined in Table I, it is possible to unambiguously assign an irreducible representation of higher symmetry to almost all of the normal modes of the four isotopomers, as shown in the second column of Tables V–VIII. The complete set of SQM quadratic force constants for the puckered conformation of cyclopentene, as evaluated in this internal coordinate representation, appears in Table IX. The corresponding force constants for the planar conformation are tabulated as supplementary material (Table XI) along with the full list of $C_s \rightarrow C_{2v}$ frequency shifts for the four isotopomers (Table XII).

The reproduction of the vibrational spectra of the cyclopentene isotopomers by the SQM force field is remarkable. Only about half of the ab initio frequencies were fitted to experimental values in the initial SQM refinement, but nearly all of the vibrational frequencies and intensities obtained with the resulting scale factors compared remarkably well with the experimental spectra. Indicative of the quality of the first set of scale factors is the fact that in the second, final refinement no computed frequency changed by more than 4 $cm^{-1}$. The positions of the 112 observed bands included in the final SQM refinement were predicted with a mean absolute percentage deviation of only 0.6% by using only 10 variable scale factors in conjunction with the DZ(d) SCF force constants. The fit to the C–H and C–D stretching fundamentals is not as good as in the other regions of the spectra; as expected,[52] the errors appear to be systematic: the scaled C–H stretching

(151) Note that in ref 16 the carbon ring of planar cyclopentene is assumed to lie in the *xz* rather than the *yz* plane. Thus, the symmetry species $b_1$ and $b_2$ in the $C_{2v}$ point group are reversed therein with respect to the convention used here.

Table V. Vibrational Assignments for Cyclopentene-$d_0$

| description of normal mode | symmetry[a] | $\nu$ (expt)[b] | $\nu$ (SQM) | $\omega$ (SCF) | infrared intensity[c] | Raman intensity[d] | $\rho$[e] | total energy distribution[f] |
|---|---|---|---|---|---|---|---|---|
| CH sym stretch | $\nu_1$ ($a_1$, a′) | 3070* (R, s) | 3071 | 3402 | 33.0 (0.32) | 137.5 (0.80) | 0.137 | $S_4(99)$ |
| CH asym stretch | $\nu_{19}$ ($b_2$, a″) | 3068* (IR, s) | 3046 | 3374 | 14.3 (0.14) | 63.8 (0.37) | 0.750 | $S_{27}(100)$ |
| $\beta$-$CH_2$ asym stretch | $\nu_2$ ($b_1$, a′) | 2963* (IR, s) | 2969 | 3289 | 93.8 (0.91) | 63.7 (0.37) | 0.739 | $S_{12}(87) + S_{13}(13)$ |
| $\alpha$-$CH_2$ asym stretch | $\nu_3$ ($b_1$, a′) | 2933* (IR, s) | 2939 | 3256 | 71.0 (0.69) | 117.0 (0.68) | 0.012 | $S_{13}(49) - S_5(28) - S_6(17) - S_{12}(5)$ |
| $\alpha$-$CH_2$ asym stretch | $\nu_{20}$ ($a_2$, a″) | [2929] (R, s) | 2936 | 3252 | 30.2 (0.29) | 114.0 (0.66) | 0.750 | $S_{19}(89) - S_{28}(11)$ |
| $\beta$-$CH_2$ sym stretch | $\nu_4$ ($a_1$, a′) | 2903* (IR, s) | 2920 | 3235 | 32.2 (0.31) | 92.3 (0.54) | 0.205 | $S_5(64) + S_{13}(28) - S_{12}(7)$ |
| $\alpha$-$CH_2$ sym stretch | $\nu_{21}$ ($b_2$, a″) | [2877] (R, m) | 2897 | 3209 | 102.8 (1.00) | 38.1 (0.22) | 0.750 | $S_{28}(89) + S_{19}(11)$ |
| $\alpha$-$CH_2$ sym stretch | $\nu_5$ ($a_1$, a′) | 2857* (R, s) | 2896 | 3208 | 30.1 (0.29) | 171.5 (1.00) | 0.135 | $S_6(83) + S_{13}(10) - S_5(7)$ |
| C=C stretch | $\nu_6$ ($a_1$, a′) | 1617* (R, s) | 1621 | 1828 | 4.01 (0.04) | 33.2 (0.19) | 0.192 | $S_1(77) - S_8(10) - S_2(6)$ |
| $\alpha$-$CH_2$ scissor | $\nu_7$ ($a_1$, a′) | 1473* (R, m) | 1482 | 1659 | 0.68 (0.01) | 5.48 (0.03) | 0.740 | $S_{10}(56) + S_9(40)$ |
| $\alpha$-$CH_2$ scissor | $\nu_{22}$ ($b_2$, a″) | [1459] (IR, m) | 1467 | 1638 | 0.41 (0.00) | 8.10 (0.05) | 0.750 | $S_{32}(89) - S_{25}(4)$ |
| $\beta$-$CH_2$ scissor | $\nu_8$ ($a_1$, a′) | 1448* (R, m) | 1455 | 1625 | 1.05 (0.01) | 14.0 (0.08) | 0.694 | $S_9(52) - S_{10}(37) + S_7(10)$ |
| CH in-plane bend | $\nu_{23}$ ($b_2$, a″) | 1353* (IR, m) | 1370 | 1515 | 1.93 (0.02) | 0.15 (0.00) | 0.750 | $S_{30}(67) + S_{25}(18) - S_{31}(8) + S_{32}(4)$ |
| $\alpha$-$CH_2$ wag | $\nu_9$ ($a_1$, a′) | 1302* (R, m) | 1310 | 1479 | 0.002 (0.00) | 2.23 (0.01) | 0.200 | $S_{11}(67) + S_2(15) - S_3(10)$ |
| $\beta$-$CH_2$ wag | $\nu_{24}$ ($b_2$, a″) | 1290† (IR, m) | 1295 | 1460 | 0.73 (0.01) | 0.71 (0.01) | 0.750 | $S_{31}(36) - S_{21}(16) + S_{33}(15) - S_{26}(12)$ |
| $\alpha$-$CH_2$ wag | $\nu_{25}$ ($b_2$, a″) | 1268 (IR, m) | 1260 | 1433 | 1.68 (0.02) | 0.20 (0.00) | 0.750 | $S_{33}(49) - S_{31}(27) - S_{30}(19)$ |
| $\beta$-$CH_2$ twist | $\nu_{26}$ ($a_2$, a″) | [1224?] (IR, m) | 1215 | 1353 | 0.080 (0.00) | 6.32 (0.04) | 0.750 | $S_{21}(53) - S_{26}(15) - S_{22}(13) - S_{29}(7)$ |
| $\alpha$-$CH_2$ twist | $\nu_{10}$ ($b_1$, a′) | 1207* (IR, m) | 1201 | 1346 | 1.73 (0.02) | 8.56 (0.05) | 0.691 | $S_{16}(77) - S_{15}(14) + S_{17}(4)$ |
| $\alpha$-$CH_2$ twist | $\nu_{27}$ ($a_2$, a″) | 1128† (IR, w) | 1122 | 1256 | 1.74 (0.02) | 1.31 (0.01) | 0.750 | $S_{22}(67) + S_{21}(12) - S_{23}(10) - S_{20}(6)$ |
| CH in-plane bend | $\nu_{11}$ ($a_1$, a′) | 1109* (R, s) | 1103 | 1221 | 0.14 (0.00) | 22.5 (0.13) | 0.455 | $S_8(81) + S_1(12)$ |
| $\alpha$-$CH_2$ rock | $\nu_{12}$ ($b_1$, a′) | 1047* (IR, s) | 1047 | 1175 | 11.5 (0.11) | 2.81 (0.02) | 0.225 | $S_{17}(48) - S_{15}(21) - S_{18}(14) - S_{16}(11)$ |
| C—C stretch | $\nu_{28}$ ($b_2$, a″) | [1030] (IR, m) | 1023 | 1123 | 2.12 (0.02) | 8.15 (0.05) | 0.750 | $S_{26}(39) + S_{33}(24) + S_{31}(16) - S_{25}(8)$ |
| C—C stretch | $\nu_{13}$ ($a_1$, a′) | 962* (R, s) | 958 | 1042 | 2.36 (0.02) | 13.2 (0.08) | 0.128 | $S_2(66) - S_{11}(19) + S_1(9)$ |
| CH out-of-plane bend | $\nu_{29}$ ($a_2$, a″) | ? | 953 | 1076 | 0.065 (0.00) | 4.67 (0.03) | 0.750 | $S_{24}(108) - S_{20}(-14)$ |
| C—C stretch | $\nu_{30}$ ($b_2$, a″) | [906] (IR, m) | 909 | 987 | 10.2 (0.10) | 0.20 (0.00) | 0.750 | $S_{25}(58) - S_{30}(12) + S_{26}(11) - S_{23}(6)$ |
| C—C stretch | $\nu_{14}$ ($a_1$, a′) | 896* (R, s) | 903 | 970 | 0.49 (0.00) | 15.8 (0.09) | 0.081 | $S_3(77) + S_{11}(7) + S_2(6)$ |
| $\alpha$-$CH_2$ rock | $\nu_{31}$ ($a_2$, a″) | 879[g] (R, m) | 874 | 965 | 0.97 (0.01) | 0.97 (0.01) | 0.750 | $S_{23}(60) + S_{21}(13) + S_{26}(10) + S_{20}(8)$ |
| $\beta$-$CH_2$ rock | $\nu_{15}$ ($b_1$, a′) | [800] (R, vw) | 802 | 888 | 1.37 (0.01) | 1.26 (0.01) | 0.643 | $S_{15}(37) - S_7(22) + S_{17}(16) - S_{18}(7)$ |
| ring shearing | $\nu_{32}$ ($b_2$, a″) | [783?] (R, vw) | 772 | 836 | 0.63 (0.01) | 3.32 (0.02) | 0.750 | $S_{29}(81) - S_{26}(10)$ |
| CH out-of-plane bend | $\nu_{16}$ ($b_1$, a′) | 695* (IR, s) | 701 | 782 | 43.3 (0.42) | 2.24 (0.01) | 0.676 | $S_{18}(64) - S_7(20) - S_{16}(5) + S_{17}(4)$ |
| ring bending | $\nu_{17}$ ($a_1$, a′) | 593† (IR, m) | 599 | 662 | 14.3 (0.14) | 1.80 (0.01) | 0.749 | $S_7(40) + S_{17}(24) + S_{15}(18) + S_{18}(14)$ |
| ring twisting | $\nu_{33}$ ($a_2$, a″) | 390* (R, w) | 387 | 419 | 0.024 (0.00) | 5.83 (0.03) | 0.750 | $S_{20}(98) - S_{24}(-11) - S_{23}(11)$ |
| ring puckering | $\nu_{18}$ ($b_1$, a′) | 127* (IR, vw) | 130 | 150 | 0.18 (0.00) | 0.61 (0.00) | 0.648 | $S_{14}(94)$ |

[a] The normal coordinates belong to the $C_s$ point group, but because the carbon framework is nearly planar, the approximate $C_{2v}$ species of each normal mode is also listed. [b] The experimental wavenumbers were taken from ref 16 unless indicated by brackets as values from ref 19. Those frequencies which were included in the first refinement of the scale factors are denoted with asterisks. Assignments for which a significant degree of uncertainty exists are highlighted by question marks; these bands were not included in the SQM fits for the scale factors. Some frequencies from ref 16 which were retained in the SQM analysis required qualitative reinterpretation, as denoted by the symbol †. The origin of each selected experimental wavenumber (IR = infrared, R = Raman) is also listed along with its relative intensity (s = strong, m = medium, w = weak, vw = very weak). [c] Computed infrared intensities in km/mol. Relative intensities shown in parentheses. [d] Computed Raman scattering activity in Å$^4$/amu. Relative values shown in parentheses. [e] Raman depolarization ratio. [f] Determined via eq 32 of the text. Each entry is listed as $S_i(n)$, where $n = 100[\mathrm{TED}]_i^k$. The signs preceding these entries denote the relative phases of the internal coordinates in the normal-mode eigenvectors. [g] Experimental value not included in either preliminary or final refinement of the scale factors.

frequencies tend to be too high, and the scaled C–D stretching frequencies too low. The source of these errors is the substantial anharmonicity of these vibrations, which is brought into prominence by the large ratio of the reduced masses ($\mu$) for C–H and C–D bond stretching. Specifically, the anharmonic contributions to the stretching fundamentals vary as $\mu^{-1}$ rather than as $\mu^{-1/2}$, as in the case of the harmonic frequencies. Thus the sizeable anharmonicities in the C–H and C–D stretches constitute significantly different percentage contributions to the fundamental frequencies, an occurrence which cannot be accounted for fully by computing harmonic frequencies with a single C–H stretch scale factor in the SQM procedure.

An integral part of the vibrational assignment tables is comprised of the total energy distributions (TEDs), by which the normal vibrations are characterized both qualitatively and quantitatively. The kinetic and potential energy distributions of normal vibration $k$ among the internal coordinates $i$ can be determined according to[141,152-154]

$$[\mathrm{KED}]_i^k = \sum_j (L_{ik} G_{ij}^{-1} L_{jk}) \tag{30}$$

and

$$[\mathrm{PED}]_i^k = \sum_j (L_{ik} F_{ij} L_{jk})/\lambda_k \tag{31}$$

where the familiar **L**, **G**, and **F** matrices are the same as those in eqs 2–4 above, and $\lambda_k$ denotes the vibrational eigenvalues appearing in eq 5. It can be readily shown[141] that the KED and PED matrices defined in this manner are, in fact, identical, thus giving rise to a composite, total energy distribution matrix which can be computed from the **L** tensor alone:

$$[\mathrm{TED}]_i^k = L_{ik} L_{ki}^{-1} \tag{32}$$

The sum of the $[\mathrm{TED}]_i^k$ values for any mode $k$ must equal 1, which facilitates the interpretation of these elements as fractional contributions to the total vibrational energy. Nevertheless, because off-diagonal interaction terms are included in the sums appearing in eqs 30 and 31, the $[\mathrm{TED}]_i^k$ elements may occasionally be negative, such as in cases where a positive, diagonal force constant for an internal coordinate is small and associated negative coupling constants are relatively large. As seen in Tables V–VIII, the ring twisting mode is the only one in cyclopentene for which a sizeable, negative TED element occurs consistently. Some authors choose to characterize normal modes by a simplified PED analysis in which the off-diagonal force constants and the $\lambda_k$ denominators in eq 31 are omitted. In our experience this method generally gives results quite similar to eq 32. However, for the ring-puckering mode of cyclopentene, the TED method appears to be superior in that 94% of the vibrational energy is ascribed to coordinate $S_{14}$ (cf. Tables I and V–VIII), as opposed to only 68% in the simplified PED analysis.

The infrared and Raman intensities presented in Tables V–VIII were evaluated on the basis of the *scaled* quadratic force field of puckered cyclopentene. In most cases the scaling procedure caused only insignificant changes in the predicted intensities. The C–H and C–D stretching intensities varied by no more than 1% upon scaling, and changes of approximately 10–20% were common for the other modes. For several relatively weak bands, the computed intensities underwent large percentage changes upon scaling which did not, however, alter their magnitudes qualitatively.

(152) Torkington, P. *J. Chem. Phys.* **1949**, *17*, 347.
(153) Morino, Y.; Kuchitsu, K. *J. Chem. Phys.* **1952**, *20*, 1809.
(154) Taylor, W. J. *J. Chem. Phys.* **1955**, *23*, 1780.

**Table VI.** Vibrational Assignments for Cyclopentene-*1*-$d_1$[a]

| description of normal mode | symmetry[b] | $\nu$ (expt) | $\nu$ (SQM) | $\omega$ (SCF) | infrared intensity | Raman intensity | $\rho$ | total energy distribution |
|---|---|---|---|---|---|---|---|---|
| CH stretch | $\nu_1$ (a′) | 3065* (IR, m) | 3059 | 3389 | 23.5 (0.23) | 102.3 (0.59) | 0.271 | $S_4(51) - S_{27}(48)$ |
| $\beta$-$CH_2$ asym stretch | $\nu_2$ (a″) | 2962* (IR, s) | 2969 | 3289 | 93.8 (0.91) | 63.6 (0.37) | 0.739 | $S_{12}(87) + S_{13}(13)$ |
| $\alpha$-$CH_2$ asym stretch | $\nu_3$ (a″) | 2939* (R, s) | 2939 | 3256 | 69.6 (0.67) | 121.6 (0.70) | 0.012 | $S_{13}(49) - S_5(28) - S_6(17) - S_{12}(5)$ |
| $\alpha$-$CH_2$ asym stretch | $\nu_4$ (a″) | 2924 (R, s) | 2936 | 3252 | 31.0 (0.30) | 113.5 (0.66) | 0.750 | $S_{19}(89) - S_{28}(11)$ |
| $\beta$-$CH_2$ sym stretch | $\nu_5$ (a′) | 2904* (R, s) | 2920 | 3235 | 31.9 (0.31) | 92.7 (0.54) | 0.203 | $S_5(64) + S_{13}(28) - S_{12}(7)$ |
| $\alpha$-$CH_2$ sym stretch | $\nu_6$ (a′) | [2866]* (R, s) | 2897 | 3209 | 103.4 (1.00) | 37.8 (0.22) | 0.718 | $S_{28}(88) + S_{19}(11)$ |
| $\alpha$-$CH_2$ sym stretch | $\nu_7$ (a′) | 2859[c] (R, s) | 2896 | 3208 | 30.4 (0.29) | 172.5 (1.00) | 0.130 | $S_6(82) + S_{13}(10) - S_5(7)$ |
| CD stretch | $\nu_8$ (a′) | 2290 (R, m) | 2268 | 2514 | 9.76 (0.09) | 38.2 (0.22) | 0.427 | $S_{27}(50) + S_4(45)$ |
| C=C stretch | $\nu_9$ (a′) | 1597* (R, s) | 1601 | 1804 | 4.65 (0.04) | 36.5 (0.21) | 0.189 | $S_1(75) - S_2(8) - S_8(8)$ |
| $\alpha$-$CH_2$ scissor | $\nu_{10}$ (a′) | 1472* (R, m) | 1482 | 1659 | 0.68 (0.01) | 5.56 (0.03) | 0.740 | $S_{10}(56) + S_9(40)$ |
| $\alpha$-$CH_2$ scissor | $\nu_{11}$ (a′) | [1458] (IR, m) | 1466 | 1638 | 0.53 (0.01) | 8.24 (0.05) | 0.749 | $S_{32}(91)$ |
| $\beta$-$CH_2$ scissor | $\nu_{12}$ (a′) | 1448* (R, m) | 1455 | 1625 | 1.03 (0.01) | 14.1 (0.08) | 0.695 | $S_9(52) - S_{10}(37) + S_7(10)$ |
| CH/CD in-plane bend | $\nu_{13}$ (a′) | 1327 (R, w) | 1332 | 1395 | 1.51 (0.01) | 2.10 (0.01) | 0.395 | $S_{30}(36) + S_{25}(20) - S_{31}(18) + S_{33}(8)$ |
| $\alpha$-$CH_2$ wag | $\nu_{14}$ (a′) | 1298 (R, m) | 1305 | 1476 | 0.26 (0.00) | 1.13 (0.01) | 0.250 | $S_{11}(63) + S_2(12) - S_3(9)$ |
| $\beta$-$CH_2$ wag | $\nu_{15}$ (a′) | ? | 1293 | 1491 | 0.78 (0.01) | 0.77 (0.00) | 0.749 | $S_{31}(34) - S_{21}(17) + S_{33}(15) - S_{26}(12)$ |
| $\alpha$-$CH_2$ wag | $\nu_{16}$ (a′) | 1257[c] (R, w) | 1239 | 1456 | 1.54 (0.01) | 2.45 (0.01) | 0.547 | $S_{33}(41) - S_{30}(32) - S_{31}(16) + S_8(6)$ |
| $\beta$-$CH_2$ twist | $\nu_{17}$ (a″) | [1207?] (IR, w) | 1213 | 1351 | 0.068 (0.00) | 6.21 (0.04) | 0.750 | $S_{21}(52) - S_{26}(15) - S_{22}(12) - S_{29}(7)$ |
| $\alpha$-$CH_2$ twist | $\nu_{18}$ (a″) | 1211* (IR, s) | 1200 | 1345 | 1.32 (0.01) | 8.62 (0.05) | 0.702 | $S_{16}(77) - S_{15}(14) + S_{17}(5)$ |
| $\alpha$-$CH_2$ twist | $\nu_{19}$ (a″) | 1137* (IR, w) | 1121 | 1255 | 1.70 (0.02) | 1.26 (0.01) | 0.749 | $S_{22}(68) + S_{21}(12) - S_{23}(10) - S_{20}(6)$ |
| $\alpha$-$CH_2$ rock | $\nu_{20}$ (a″) | 1044* (IR, s) | 1042 | 1170 | 8.85 (0.09) | 3.08 (0.02) | 0.239 | $S_{17}(47) - S_{15}(21) - S_{16}(12) - S_{18}(12)$ |
| C—C stretch | $\nu_{21}$ (a′) | 1029 (R, m) | 1028 | 1129 | 2.94 (0.03) | 9.40 (0.05) | 0.631 | $S_{26}(29) + S_{33}(25) - S_{25}(13) + S_{31}(11)$ |
| CH/CD in-plane bend | $\nu_{22}$ (a′) | 978 (R, s) | 977 | 1069 | 2.47 (0.02) | 16.0 (0.09) | 0.287 | $S_8(31) + S_{26}(18) + S_{25}(16) + S_{31}(8)$ |
| C—C stretch | $\nu_{23}$ (a′) | 952* (R, m) | 950 | 1035 | 2.98 (0.03) | 10.2 (0.06) | 0.175 | $S_2(57) - S_{11}(20) + S_1(8)$ |
| C—C stretch | $\nu_{24}$ (a′) | 899* (R, s) | 903 | 972 | 1.36 (0.01) | 15.7 (0.09) | 0.085 | $S_3(70) + S_{11}(6) + S_2(6) - S_{25}(4)$ |
| CH/CD out-of-plane bend | $\nu_{25}$ (a″) | 893[†] (IR, w) | 894 | 1005 | 2.49 (0.02) | 4.89 (0.03) | 0.728 | $S_{24}(49) - S_{23}(31) - S_{21}(8) - S_{22}(7)$ |
| $\alpha,\beta$-$CH_2$ rock | $\nu_{26}$ (a″) | 855 (IR, s) | 858 | 957 | 4.69 (0.05) | 1.65 (0.01) | 0.744 | $S_{24}(42) + S_{23}(34) + S_{21}(5) - S_{18}(5)$ |
| ring mode | $\nu_{27}$ (a′) | [802] (R, w) | 815 | 894 | 2.58 (0.02) | 2.95 (0.02) | 0.750 | $S_{25}(19) - S_7(19) + S_{15}(17) - S_{30}(14)$ |
| $\alpha,\beta$-$CH_2$ rock | $\nu_{28}$ (a″ + a′) | [779?] (R, w) | 772 | 847 | 0.74 (0.01) | 1.04 (0.01) | 0.743 | $S_{29}(19) - S_8(16) - S_{15}(14) - S_{17}(11)$ |
| ring shearing | $\nu_{29}$ (a′) | 750 (R, m) | 750 | 814 | 3.47 (0.03) | 2.67 (0.02) | 0.716 | $S_{29}(58) + S_8(13) - S_{26}(12) + S_{30}(4)$ |
| ring bending | $\nu_{30}$ (a′ + a″) | 630[†] (R, vw) | 638 | 705 | 7.99 (0.08) | 1.89 (0.01) | 0.705 | $S_7(42) - S_{18}(23) + S_{15}(14) - S_{24}(6)$ |
| CH/CD out-of-plane bend | $\nu_{31}$ (a″) | 565* (IR, s) | 561 | 627 | 31.8 (0.31) | 1.89 (0.01) | 0.736 | $S_{18}(54) + S_{17}(18) + S_7(13) + S_{24}(7)$ |
| ring twisting | $\nu_{32}$ (a″) | 369* (R, w) | 371 | 402 | 0.46 (0.00) | 4.53 (0.03) | 0.750 | $S_{20}(100) - S_{24}(-14) - S_{23}(10)$ |
| ring puckering | $\nu_{33}$ (a″) | 126* (IR, vw) | 129 | 149 | 0.16 (0.00) | 0.58 (0.00) | 0.644 | $S_{14}(95)$ |

[a] See footnotes *b–f* of Table V. [b] The normal coordinates have no symmetry, but because the carbon framework is nearly planar, the approximate $C_s$ species of each is listed. Note that the plane of symmetry being referred to *yz* (see Figure 1). Some modes cannot be characterized by a single $C_s$-symmetry species. [c] Experimental value not included in either preliminary or final refinement of the scale factors.

**Table VII.** Vibrational Assignments for Cyclopentene-*1,2,3,3-d*$_4$[a]

| description of normal mode | symmetry | $\nu$ (expt) | $\nu$ (SQM) | $\omega$ (SCF) | infrared intensity | Raman intensity | $\rho$ | total energy distribution |
|---|---|---|---|---|---|---|---|---|
| $\beta$-$CH_2$ asym stretch | $\nu_1$ (a″) | 2969* (R, s) | 2966 | 3286 | 71.0 (1.00) | 66.0 (0.61) | 0.726 | $S_{12}(92)$ |
| $\alpha$-$CH_2$ asym stretch | $\nu_2$ (a″) | [2916?] (R, s) | 2938 | 3254 | 61.4 (0.86) | 107.2 (0.99) | 0.208 | $S_{13}(32) + S_{19}(32) - S_5(19) - S_6(7)$ |
| $\beta$-$CH_2$ sym stretch | $\nu_3$ (a′) | 2905* (R, s) | 2922 | 3237 | 37.6 (0.53) | 106.1 (0.98) | 0.196 | $S_5(77) + S_{19}(10) + S_{13}(9) - S_{12}(5)$ |
| $\alpha$-$CH_2$ sym stretch | $\nu_4$ (a′) | 2861* (R, s) | 2896 | 3208 | 65.8 (0.93) | 108.0 (1.00) | 0.192 | $S_{28}(43) + S_6(43) + S_{19}(5) + S_{13}(5)$ |
| CD sym stretch | $\nu_5$ (a′) | 2313* (R, m) | 2289 | 2539 | 14.9 (0.21) | 47.5 (0.44) | 0.216 | $S_4(94) - S_1(6)$ |
| CD asym stretch | $\nu_6$ (a′) | 2265* (R, m) | 2247 | 2488 | 5.65 (0.08) | 31.5 (0.29) | 0.748 | $S_{27}(98)$ |
| $\alpha$-$CD_2$ asym stretch | $\nu_7$ (a″) | 2194* (R, m) | 2179 | 2414 | 28.9 (0.41) | 40.4 (0.37) | 0.713 | $S_{19}(48) - S_{13}(48)$ |
| $\alpha$-$CD_2$ sym stretch | $\nu_8$ (a′) | [2113]* (R, s) | 2114 | 2341 | 36.0 (0.51) | 71.3 (0.66) | 0.139 | $S_{28}(48) - S_6(48)$ |
| C=C stretch | $\nu_9$ (a′) | 1580* (R, s) | 1579 | 1778 | 5.55 (0.08) | 39.6 (0.37) | 0.199 | $S_1(76) - S_2(10) - S_8(5) + S_4(4)$ |
| $\alpha,\beta$-$CH_2$ scissor | $\nu_{10}$ (a′) | 1467* (R, m) | 1477 | 1652 | 0.79 (0.01) | 4.90 (0.05) | 0.749 | $S_9(43) + S_{10}(28) + S_{32}(24)$ |
| $\alpha,\beta$-$CH_2$ scissor | $\nu_{11}$ (a′) | 1452* (R, s) | 1458 | 1628 | 0.99 (0.01) | 11.5 (0.11) | 0.700 | $S_9(49) - S_{32}(22) - S_{10}(19) + S_7(7)$ |
| $\alpha,\beta$-$CH_2$ wag | $\nu_{12}$ (a′) | [1310] (R, vw) | 1302 | 1476 | 0.96 (0.01) | 0.79 (0.01) | 0.477 | $S_{31}(32) - S_{11}(17) - S_{33}(17) - S_{25}(16)$ |
| $\beta$-$CH_2$ wag | $\nu_{13}$ (a′) | 1290 (R, vw) | 1289 | 1458 | 0.61 (0.01) | 0.54 (0.01) | 0.691 | $S_{31}(37) + S_{11}(15) - S_{26}(12) + S_{33}(11)$ |
| $\beta$-$CH_2$ twist | $\nu_{14}$ (a″ + a′) | [1236] (IR, vw) | 1236 | 1372 | 0.070 (0.00) | 3.01 (0.03) | 0.710 | $S_{21}(25) + S_{11}(18) - S_{25}(17) - S_{30}(10)$ |
| C—C stretch/$\beta$-$CH_2$ twist | $\nu_{15}$ (a′ + a″) | 1211 (R, vw) | 1202 | 1319 | 0.45 (0.01) | 3.77 (0.03) | 0.748 | $S_{21}(27) - S_{26}(18) + S_{25}(15) + S_{30}(8)$ |
| $\alpha$-$CH_2$ twist | $\nu_{16}$ (a″) | 1160† (R, w) | 1152 | 1288 | 1.43 (0.02) | 4.62 (0.04) | 0.648 | $S_{16}(38) + S_{21}(21) + S_{22}(17) - S_{15}(8)$ |
| CD in-plane bend | $\nu_{17}$ (a′) | 1100† (R, w) | 1115 | 1238 | 2.62 (0.04) | 2.75 (0.03) | 0.514 | $S_{30}(16) + S_{10}(14) - S_{33}(13) - S_{32}(10)$ |
| $\alpha$-$CD_2$ scissor | $\nu_{18}$ (a′) | 1085* (R, m) | 1085 | 1207 | 0.45 (0.01) | 5.05 (0.05) | 0.234 | $S_{32}(28) + S_{30}(17) - S_{10}(17) - S_{33}(13)$ |
| $\alpha,\beta$-$CH_2$ rock | $\nu_{19}$ (a″) | 1041†/[b] (IR, s) | 1037 | 1162 | 2.69 (0.04) | 2.60 (0.02) | 0.517 | $S_{17}(32) - S_{15}(30) - S_{22}(15) + S_{23}(9)$ |
| C—C stretch/$\alpha,\beta$-$CH_2$ wag | $\nu_{20}$ (a′) | 985* (R, w) | 983 | 1076 | 0.63 (0.01) | 6.54 (0.06) | 0.720 | $S_{26}(36) + S_{33}(18) + S_3(15) + S_{31}(13)$ |
| C—C stretch | $\nu_{21}$ (a′) | 910* (R, s) | 905 | 987 | 1.04 (0.01) | 31.8 (0.29) | 0.108 | $S_2(38) + S_3(22) + S_1(10) + S_{10}(7)$ |
| $\alpha$-$CD_2$ twist | $\nu_{22}$ (a″) | 875† (R, m) | 869 | 969 | 4.94 (0.07) | 6.88 (0.06) | 0.622 | $S_{16}(25) - S_{24}(16) + S_{23}(14) - S_{22}(12)$ |
| $\alpha,\beta$-$CH_2/CD_2$ rock | $\nu_{23}$ (a″) | [840] (R, w) | 842 | 935 | 0.87 (0.01) | 2.02 (0.02) | 0.516 | $S_{15}(18) - S_7(13) + S_{23}(13) + S_{22}(12)$ |
| $\alpha$-$CD_2$ wag/C—C stretch | $\nu_{24}$ (a′) | 825† (R, m) | 812 | 894 | 1.82 (0.03) | 2.69 (0.02) | 0.459 | $S_{11}(19) + S_3(19) + S_{30}(13) - S_{26}(11)$ |
| CD in-plane bend | $\nu_{25}$ (a′) | 802† (R, w) | 794 | 876 | 0.45 (0.01) | 6.28 (0.06) | 0.749 | $S_8(49) + S_{23}(13) + S_{22}(9) + S_7(7)$ |
| ring shearing | $\nu_{26}$ (a′) | [771] (IR, w) | 768 | 841 | 0.68 (0.01) | 4.88 (0.05) | 0.720 | $S_{29}(45) - S_{24}(15) + S_{25}(13) + S_{11}(5)$ |
| CD out-of-plane bend | $\nu_{27}$ (a″) | 726† (R, w) | 729 | 812 | 3.73 (0.05) | 2.45 (0.02) | 0.721 | $S_{24}(42) + S_{25}(14) - S_{30}(12) - S_{33}(11)$ |
| ring mode | $\nu_{28}$ (a′) | 715 (IR, vw) | 714 | 785 | 1.55 (0.02) | 0.82 (0.01) | 0.548 | $S_8(17) + S_{29}(15) - S_7(12) - S_3(9)$ |
| $\alpha$-$CD_2$ rock | $\nu_{29}$ (a″) | [700] (IR, m) | 700 | 775 | 2.17 (0.03) | 1.08 (0.01) | 0.734 | $S_{24}(34) + S_{29}(18) + S_{23}(17) + S_7(7)$ |
| ring bending | $\nu_{30}$ (a′) | 604 (R, w) | 601 | 666 | 5.10 (0.07) | 1.29 (0.01) | 0.669 | $S_7(33) - S_{18}(20) + S_{15}(18) + S_{16}(9)$ |
| CD out-of-plane bend | $\nu_{31}$ (a″) | 502* (IR, s) | 501 | 561 | 29.6 (0.42) | 0.88 (0.01) | 0.716 | $S_{18}(65) + S_{17}(20) + S_7(6)$ |
| ring twisting | $\nu_{32}$ (a″) | 338* (R, m) | 338 | 366 | 0.10 (0.00) | 3.87 (0.04) | 0.750 | $S_{20}(96) - S_{24}(-14) - S_{23}(13)$ |
| ring puckering | $\nu_{33}$ (a″) | 120* (IR, vw) | 120 | 139 | 0.13 (0.00) | 0.51 (0.00) | 0.645 | $S_{14}(94)$ |

[a] See footnote *b* of Table VI and footnotes *b–f* of Table V. [b] Experimental value not included in either preliminary or final refinement of the scale factors.

Table VIII. Vibrational Assignments for Cyclopentene-$d_8$[a]

| description of normal mode | symmetry | $\nu$ (expt) | $\nu$ (SQM) | $\omega$ (SCF) | infrared intensity | Raman intensity | $\rho$ | total energy distribution |
|---|---|---|---|---|---|---|---|---|
| CD sym stretch | $\nu_1$ ($a_1$, a′) | 2305* (R, s) | 2289 | 2539 | 13.0 (0.22) | 52.4 (0.54) | 0.188 | $S_4(93) - S_1(6)$ |
| CD asym stretch | $\nu_{19}$ ($b_2$, a″) | 2268* (R, s) | 2247 | 2488 | 6.44 (0.11) | 30.7 (0.32) | 0.750 | $S_{27}(98)$ |
| $\beta$-$CD_2$ asym stretch | $\nu_2$ ($b_1$, a′) | 2230* (IR, s) | 2204 | 2441 | 44.1 (0.74) | 31.4 (0.32) | 0.746 | $S_{12}(93) + S_{13}(6)$ |
| $\alpha$-$CD_2$ asym stretch | $\nu_3$ ($b_1$, a′) | 2202* (R, s) | 2178 | 2114 | 36.7 (0.62) | 16.3 (0.17) | 0.354 | $S_{13}(89) - S_{12}(6)$ |
| $\alpha$-$CD_2$ asym stretch | $\nu_{20}$ ($a_2$, a″) | 2202[b] (R, s) | 2177 | 2412 | 6.83 (0.12) | 64.7 (0.67) | 0.750 | $S_{19}(97)$ |
| $\beta$-$CD_2$ sym stretch | $\nu_4$ ($a_1$, a′) | 2145* (R, s) | 2136 | 2365 | 31.9 (0.54) | 97.3 (1.00) | 0.044 | $S_5(81) + S_6(15)$ |
| $\alpha$-$CD_2$ sym stretch | $\nu_{21}$ ($b_2$, a″) | 2138* (IR, m) | 2113 | 2340 | 59.4 (1.00) | 16.8 (0.17) | 0.750 | $S_{28}(96)$ |
| $\alpha$-$CD_2$ sym stretch | $\nu_5$ ($a_1$, a′) | 2100* (R, s) | 2111 | 2338 | 11.1 (0.19) | 76.0 (0.78) | 0.190 | $S_6(80) - S_5(17)$ |
| C=C stretch | $\nu_6$ ($a_1$, a′) | 1577* (R, s) | 1577 | 1774 | 5.68 (0.10) | 39.3 (0.40) | 0.206 | $S_1(76) - S_2(10) - S_8(5) + S_4(4)$ |
| C—C stretch | $\nu_{22}$ ($b_2$, a″) | ? | 1237 | 1346 | 0.13 (0.00) | 0.33 (0.00) | 0.750 | $S_{25}(56) + S_{30}(29) + S_{33}(8)$ |
| C—C stretch | $\nu_{23}$ ($b_2$, a″) | ? | 1194 | 1302 | 1.04 (0.02) | 2.83 (0.03) | 0.750 | $S_{26}(58) - S_{31}(17) - S_{29}(14) - S_{32}(5)$ |
| C—C stretch | $\nu_7$ ($a_1$, a′) | 1190 (R, vw) | 1191 | 1311 | 1.69 (0.03) | 1.24 (0.01) | 0.209 | $S_3(33) - S_{11}(31) - S_2(22) - S_7(5)$ |
| $\alpha$-$CD_2$ scissor | $\nu_8$ ($a_1$, a′) | 1113* (R, m) | 1121 | 1246 | 0.02 (0.00) | 7.40 (0.08) | 0.093 | $S_{10}(56) - S_9(17) - S_2(11) - S_3(7)$ |
| $\beta$-$CD_2$ scissor | $\nu_9$ ($a_1$, a′) | 1070* (IR, m) | 1066 | 1191 | 0.41 (0.01) | 2.47 (0.03) | 0.712 | $S_9(59) - S_{10}(17) + S_7(14) - S_{11}(6)$ |
| $\alpha$-$CD_2$ scissor | $\nu_{24}$ ($b_2$, a″) | 1062* (IR, m) | 1058 | 1186 | 0.53 (0.01) | 1.45 (0.01) | 0.750 | $S_{32}(79) + S_{30}(8) - S_{31}(7)$ |
| $\alpha,\beta$-$CD_2$ wag | $\nu_{25}$ ($b_2$, a″) | [998] (R, vw) | 1003 | 1137 | 0.70 (0.01) | 0.01 (0.00) | 0.750 | $S_{33}(41) - S_{30}(33) - S_{31}(25)$ |
| $\alpha,\beta$-$CD_2$ rock | $\nu_{10}$ ($b_1$, a′) | [962?] (R, w) | 949 | 1064 | 0.69 (0.01) | 3.22 (0.03) | 0.399 | $S_{15}(34) - S_{16}(28) - S_{17}(26) + S_{14}(5)$ |
| $\beta$-$CD_2$ twist | $\nu_{26}$ ($a_2$, a″) | 930† (R, w) | 923 | 1031 | 0.08 (0.00) | 0.62 (0.01) | 0.750 | $S_{21}(55) - S_{23}(25) - S_{20}(7)$ |
| $\alpha$-$CD_2$ twist | $\nu_{27}$ ($a_2$, a″) | [887?] (R, vw) | 883 | 988 | 1.69 (0.03) | 9.40 (0.10) | 0.750 | $S_{22}(55) + S_{24}(21) - S_{21}(8) - S_{23}(6)$ |
| C—C stretch | $\nu_{11}$ ($a_1$, a′) | 878 (R, s) | 868 | 939 | 2.12 (0.04) | 29.6 (0.30) | 0.131 | $S_2(30) + S_3(15) + S_{10}(13) + S_8(11)$ |
| $\alpha$-$CD_2$ twist | $\nu_{12}$ ($b_1$, a′) | 849† (IR, s) | 843 | 956 | 8.53 (0.14) | 6.12 (0.06) | 0.473 | $S_{16}(42) - S_{17}(25) + S_{18}(16) + S_8(5)$ |
| CD in-plane bend | $\nu_{13}$ ($a_1$, a′) | 790† (R, m) | 785 | 859 | 0.25 (0.00) | 8.17 (0.08) | 0.598 | $S_8(57) - S_2(14) + S_7(10) - S_9(6)$ |
| $\alpha,\beta$-$CD_2$ wag | $\nu_{28}$ ($b_2$, a″) | [764?] (IR, w) | 773 | 862 | 0.23 (0.00) | 8.47 (0.09) | 0.750 | $S_{26}(25) - S_{29}(22) + S_{31}(20) + S_{33}(19)$ |
| ring shearing | $\nu_{29}$ ($b_2$, a″) | 750 (R, m) | 747 | 827 | 0.17 (0.00) | 0.52 (0.01) | 0.750 | $S_{29}(29) + S_{31}(26) + S_{25}(8) - S_{24}(8)$ |
| $\alpha$-$CD_2$ wag | $\nu_{14}$ ($a_1$, a′) | 724? (IR, m) | 732 | 814 | 1.12 (0.02) | 2.07 (0.02) | 0.482 | $S_{11}(53) + S_3(31) - S_2(6)$ |
| CD out-of-plane bend | $\nu_{30}$ ($a_2$, a″) | [716?] (IR, w) | 720 | 806 | 3.39 (0.06) | 2.20 (0.02) | 0.750 | $S_{24}(50) - S_{22}(15) + S_{25}(14) - S_{33}(11)$ |
| ring mode | $\nu_{31}$ ($a_2 + b_2$, a″) | 709 (IR, w) | 708 | 776 | 5.26 (0.09) | 0.86 (0.01) | 0.750 | $S_{22}(19) - S_{29}(18) - S_{24}(17) + S_{25}(13)$ |
| ring bending | $\nu_{15}$ ($a_1$, a′) | [693] (R, w) | 680 | 747 | 0.10 (0.00) | 1.25 (0.01) | 0.572 | $S_7(41) - S_8(20) - S_{15}(11) + S_{10}(9)$ |
| $\alpha$-$CD_2$ rock | $\nu_{32}$ ($a_2$, a″) | ? | 649 | 724 | 0.12 (0.00) | 0.05 (0.00) | 0.750 | $S_{23}(41) + S_{21}(26) + S_{24}(10) + S_{29}(8)$ |
| CD out-of-plane bend | $\nu_{16}$ ($b_1$, a′) | 543* (IR, s) | 544 | 609 | 15.4 (0.26) | 1.10 (0.01) | 0.673 | $S_{18}(50) - S_{15}(22) - S_{16}(16) - S_7(9)$ |
| $\alpha,\beta$-$CD_2$ rock | $\nu_{17}$ ($b_1$, a′) | 465* (IR, s) | 456 | 509 | 15.7 (0.26) | 0.79 (0.01) | 0.742 | $S_{17}(35) + S_{18}(31) + S_{15}(21) + S_7(11)$ |
| ring twisting | $\nu_{33}$ ($a_2$, a″) | 317* (R, w) | 320 | 347 | 0.005 (0.00) | 4.10 (0.04) | 0.750 | $S_{20}(93) - S_{23}(17) - S_{24}(-13)$ |
| ring puckering | $\nu_{18}$ ($b_1$, a′) | 108* (IR, vw) | 103 | 119 | 0.11 (0.00) | 0.41 (0.00) | 0.654 | $S_{14}(93)$ |

[a] See footnotes *a–f* of Table V. [b] Experimental value not included in either preliminary or final refinement of scale factors.

For example, the computed IR intensity of the $\nu_9$ band of cyclopentene-$d_0$ changed from 0.02 to 0.002 km/mol upon scaling of the force constants, and the Raman intensity of the $\nu_{16}$ band of cyclopentene-$d_1$ increased from 1.18 to 2.45 Å$^4$/amu. Only a few computed intensities experienced alterations which were qualitatively significant, as indicated in each case by large changes in the associated TED. In particular, in the Raman spectrum of cyclopentene-$d_8$, the intensity of the $\nu_{29}$ band decreased from 2.72 to 0.52 Å$^4$/amu, whereas the intensities of the $\nu_{11}$ and $\nu_{12}$ modes, which were strongly coupled before scaling but much less so afterward, changed from 18.0 and 15.4 to 29.6 and 6.1 Å$^4$/amu, respectively.

The extensive experimental work on the vibrational spectrum of cyclopentene by Villarreal, Laane, Bush, and Harris (VLBH)[16] provides the groundwork for the final SQM assignments presented in Tables V–VIII. While the SQM study reported here confirms large portions of the analysis by VLBH, numerous reassignments have been made which deserve comment. In general, SQM frequency predictions which do not involve hydrogen stretches are reliable to within 20 cm$^{-1}$, and this expectation provides a criterion for suggesting reinterpretations of experimental bands. In Tables V–VIII several new assignments of bands previously tabulated by Villarreal[19] are made which are reasonable on the basis of the SQM data alone. Codes are used in the vibrational assignment tables to highlight these changes, as detailed in footnote *b* of Table V. Obviously, further investigation of the appropriate regions of the experimental spectra is necessary to confirm or readjust the precise wavenumber assignments.

In cyclopentene-$d_0$, 22 of the assignments of VLBH[16] were retained in the SQM analysis without modification. One minor reassignment involved alterations of the $\nu_{20}$ and $\nu_{21}$ C–H stretching fundamentals to bands listed in Villarreal's thesis[19] at 2929 and 2877 cm$^{-1}$, respectively, as suggested by the SQM ordering and depolarization data. Similarly, $\nu_{22}$ was changed from 1438 to 1459 cm$^{-1}$ to match the computed ordering of the $CH_2$-scissoring fundamentals. Other reassignments entailed the selection of two medium IR bands[19] at 1030 and 906 cm$^{-1}$, as well as two very weak Raman bands[19] at 800 and 783 cm$^{-1}$, for assignment to $\nu_{28}$, $\nu_{30}$, $\nu_{15}$, and $\nu_{32}$, respectively. Because the predicted IR and Raman intensities of $\nu_{14}$ and $\nu_{30}$ are complementary, the infrared absorption near 900 cm$^{-1}$ and the strong Raman band at 896 cm$^{-1}$, which are jointly ascribed to a ring-mode fundamental by VLBH, apparently arise from different modes. The $\beta$-$CH_2$ twist, $\nu_{26}$, which is formally infrared forbidden in planar cyclopentene, is tentatively assigned to a medium IR band[19] at 1224 cm$^{-1}$, although it may in fact be coincident with $\nu_{10}$ in the Raman spectrum[16] near 1209 cm$^{-1}$. In addition, the $\beta$-$CH_2$ wag, $\nu_{24}$, is altered from the 1128-cm$^{-1}$ value of VLBH to the broad IR band observed[16] at 1290 cm$^{-1}$, which is assumed to be distinct from the nearby Raman band at 1302 cm$^{-1}$. Consequently the 1128-cm$^{-1}$ band is reassigned to $\nu_{27}$($\alpha$-$CH_2$ twist). The assignments by VLBH of bands at 933, 695, and 608 cm$^{-1}$ to ring-mode fundamentals were reinterpreted on the basis of the SQM data. First, no clear correlation is present between the very weak Raman band at 933 cm$^{-1}$ and an appropriate SQM fundamental frequency. The band might be due to the asymmetric CH out-of-plane bend, which cannot lie at 1047 cm$^{-1}$ as proposed by VLBH; however, this association is tenuous because the predicted Raman intensity for $\nu_{29}$ is sizeable. Second, no ring modes contribute to the IR absorptions near 700 cm$^{-1}$; the strong band at 695 cm$^{-1}$ is attributable only to $\nu_{16}$, the symmetric CH out-of-plane bend. Finally, the 608-cm$^{-1}$ shoulder reported by VLBH does not appear to be distinct from the medium IR band at 593 cm$^{-1}$, which is best described as a strong mixture of ring bending and $\alpha,\beta$-$CH_2$ rocking.

In the spectrum of cyclopentene-*1*-$d_1$, 25 assignments from VLBH were found to be in agreement with the results of the SQM analysis. As before, an $\alpha$-$CH_2$ scissoring fundamental was altered from a shoulder at 1435 cm$^{-1}$ to a broad IR feature[19] at 1458 cm$^{-1}$, in order to match the SQM frequency ordering. The $\beta$-$CH_2$ wag, $\nu_{15}$, was assigned by VLBH to 1121 cm$^{-1}$, at variance with the location of this band at 1293 cm$^{-1}$ in the SQM spectrum. The close proximity of $\nu_{14}$ and $\nu_{15}$ precludes a precise assignment for the latter. An IR shoulder at 1207 cm$^{-1}$ ascribed by VLBH to a $CH_2$ twist is tentatively matched with $\nu_{17}$; yet the predicted intensity suggests that this band should not be directly observable in the infrared. According to VLBH, the asymmetric CH/CD out-of-plane bend, $\nu_{25}$, overlaps both a $CH_2$ rock and a ring-mode absorption near 1040 cm$^{-1}$; however, the TEDs in Table VI reveal

**Table IX.** Final SQM Quadratic Force Constant Matrix for Puckered ($C_s$) Cyclopentene[a]

A′ Symmetry Vibrational Modes

| | $j$ = | | | | | | | | | | | | | | | | | |
|---|---|---|---|---|---|---|---|---|---|---|---|---|---|---|---|---|---|---|
| $i$ | 1 | 2 | 3 | 4 | 5 | 6 | 7 | 8 | 9 | 10 | 11 | 12 | 13 | I4 | 15 | 16 | 17 | 18 |
| 1 | 8.5551 | | | | | | | | | | | | | | | | | |
| 2 | 0.3015 | 4.6267 | | | | | | | | | | | | | | | | |
| 3 | −0.0304 | 0.0309 | 4.3385 | | | | | | | | | | | | | | | |
| 4 | 0.1091 | 0.0541 | −0.0389 | 5.1322 | | | | | | | | | | | | | | |
| 5 | −0.0467 | −0.0173 | 0.1328 | 0.0064 | 4.8127 | | | | | | | | | | | | | |
| 6 | −0.0218 | 0.1082 | 0.0947 | 0.0181 | 0.0262 | 4.7480 | | | | | | | | | | | | |
| 7 | 0.2107 | −0.3129 | 0.0882 | −0.0467 | −0.1464 | 0.1723 | 1.7255 | | | | | | | | | | | |
| 8 | 0.0910 | −0.2268 | 0.1938 | 0.0002 | −0.0099 | −0.0064 | 0.2387 | 0.8642 | | | | | | | | | | |
| 9 | 0.3532 | 0.2433 | −0.1141 | 0.0108 | −0.2406 | 0.0075 | 0.5921 | −0.0217 | 2.5854 | | | | | | | | | |
| 10 | 0.1731 | 0.3188 | 0.0843 | 0.0155 | 0.0059 | −0.2350 | −0.6260 | 0.0267 | 0.0253 | 2.4533 | | | | | | | | |
| 11 | 0.0160 | −0.1762 | 0.1925 | −0.0077 | 0.0077 | −0.0141 | 0.0201 | −0.0307 | 0.0038 | 0.0091 | 0.6068 | | | | | | | |
| 12 | −0.0072 | 0.0034 | −0.0066 | 0.0004 | 0.0175 | 0.0039 | −0.0386 | −0.0029 | −0.0087 | −0.0027 | −0.0088 | 4.7229 | | | | | | |
| 13 | −0.0135 | 0.0239 | 0.0224 | −0.0021 | −0.0080 | −0.0398 | −0.0217 | −0.0046 | 0.0043 | 0.0045 | 0.0004 | 0.0319 | 4.6318 | | | | | |
| 14 | 0.0500 | 0.0696 | −0.0921 | −0.0018 | 0.0041 | −0.0036 | −0.0096 | 0.0090 | 0.0562 | 0.0704 | −0.0161 | 0.0099 | 0.0042 | 0.0510 | | | | |
| 15 | 0.0169 | 0.0631 | 0.0141 | 0.0052 | −0.0204 | −0.0175 | −0.0376 | −0.0141 | 0.1044 | −0.0145 | −0.0108 | 0.1050 | −0.0393 | 0.0408 | 0.6225 | | | |
| 16 | −0.0084 | −0.0181 | 0.0425 | −0.0018 | 0.0056 | −0.0007 | −0.0296 | 0.0096 | 0.0242 | −0.0126 | 0.0072 | −0.0374 | −0.0121 | 0.0008 | −0.0651 | 0.6029 | | |
| 17 | −0.0360 | 0.0138 | −0.0609 | −0.0018 | 0.0218 | 0.0089 | −0.0523 | −0.0109 | 0.0079 | −0.0472 | −0.0154 | −0.0413 | 0.1245 | −0.0249 | −0.0261 | 0.0097 | 0.5796 | |
| 18 | 0.0054 | −0.0183 | −0.0028 | 0.0056 | −0.0046 | 0.0024 | −0.0055 | −0.0164 | 0.0047 | −0.0085 | 0.0063 | −0.0014 | −0.0175 | −0.0154 | −0.0069 | 0.0512 | −0.0517 | 0.3132 |

A″ Symmetry Vibrational Modes

| | $j$ = | | | | | | | | | | | | | | |
|---|---|---|---|---|---|---|---|---|---|---|---|---|---|---|---|
| $i$ | 19 | 20 | 21 | 22 | 23 | 24 | 25 | 26 | 27 | 28 | 29 | 30 | 31 | 32 | 33 |
| 19 | 4.6293 | | | | | | | | | | | | | | |
| 20 | 0.0276 | 0.3229 | | | | | | | | | | | | | |
| 21 | −0.0356 | −0.0135 | 0.6259 | | | | | | | | | | | | |
| 22 | −0.0179 | −0.0623 | −0.0720 | 0.6109 | | | | | | | | | | | |
| 23 | 0.1229 | 0.0534 | −0.0519 | 0.0130 | 0.6137 | | | | | | | | | | |
| 24 | 0.0141 | 0.2699 | −0.0069 | −0.0278 | 0.0352 | 0.5108 | | | | | | | | | |
| 25 | 0.0125 | 0.0213 | −0.0021 | −0.0085 | 0.0305 | 0.0245 | 4.6093 | | | | | | | | |
| 26 | 0.0067 | 0.0603 | −0.0700 | 0.0061 | −0.0236 | 0.0328 | 0.1119 | 4.1641 | | | | | | | |
| 27 | −0.0013 | 0.0019 | 0.0040 | −0.0046 | 0.0034 | 0.0050 | 0.0559 | 0.0445 | 5.1038 | | | | | | |
| 28 | −0.0376 | 0.0131 | −0.0021 | 0.0024 | 0.0116 | 0.0045 | 0.2235 | 0.1051 | 0.0062 | 4.7391 | | | | | |
| 29 | −0.0121 | 0.0245 | −0.0399 | 0.0231 | −0.0016 | 0.0056 | 0.2415 | −0.3542 | −0.1693 | 0.1202 | 1.6132 | | | | |
| 30 | −0.0030 | −0.0034 | −0.0129 | 0.0028 | −0.0054 | −0.0178 | −0.2534 | −0.0810 | 0.0148 | −0.0182 | 0.3594 | 0.9042 | | | |
| 31 | 0.0108 | 0.0032 | −0.0423 | 0.0303 | 0.0031 | 0.0006 | −0.0201 | 0.3286 | 0.0063 | 0.0076 | −0.0581 | −0.0226 | 0.6022 | | |
| 32 | 0.0012 | −0.0253 | −0.0261 | −0.0091 | −0.0374 | 0.0058 | −0.3359 | −0.2166 | −0.0057 | −0.2546 | −0.3794 | 0.0037 | 0.0053 | 2.4167 | |
| 33 | 0.0012 | 0.0043 | −0.0333 | 0.0143 | −0.0040 | −0.0001 | −0.1659 | 0.2304 | 0.0021 | −0.0199 | −0.0826 | −0.0008 | 0.0271 | −0.0043 | 0.5771 |

[a] Relative to the symmetrized internal coordinates $S_1$–$S_{33}$ defined in Table I. Units are consistent with energy measured in aJ, bond lengths in Å, and angles in rad.

that the weak IR band observed at 893 $cm^{-1}$ is attributable to this out-of-plane bend rather than a ring mode, as originally assigned.[16] The missing ring-mode absorption may correspond to a previously unassigned, depolarized Raman band[19] at 802 $cm^{-1}$. Additional points of concern in Table VI are the assignment of $\nu_{28}$ to a weak, polarized Raman band[19] at 779 $cm^{-1}$, which is uncertain due to the corresponding theoretical prediction of a large depolarization ratio, and the characterization of the Raman band at 630 $cm^{-1}$ as a ring-bending rather than $CH_2$-rocking fundamental. Finally, the SQM analysis shows that the 708- and 600-$cm^{-1}$ bands listed by VLBH are not attributable to fundamental frequencies of cyclopentene-$d_1$.

Of the 17 vibrational modes of cyclopentene-*1,2,3,3*-$d_4$ which were not assigned experimental frequencies in the first refinement of the scale factors, most were later correlated with observed bands which were previously misassigned or left unassigned. The $\alpha$-$CH_2$ asymmetric stretch, $\nu_2$, was assigned by VLBH to a shoulder in the IR spectrum at 2941 $cm^{-1}$, but other possibilities are the strong, polarized Raman band[19] at 2954 $cm^{-1}$ and a similar band of unknown polarization[19] at 2916 $cm^{-1}$. On the basis of the tendency of the SQM procedure to overestimate C–H stretching frequencies, $\nu_2$ is tentatively assigned to the 2916-$cm^{-1}$ band. Weak infrared and Raman bands listed in Villarreal's thesis at 1310, 1236, 840, and 700 $cm^{-1}$ seem to correlate best with SQM predictions for the $CH_2/CD_2$ wagging, twisting, and rocking modes $\nu_{12}$, $\nu_{14}$, $\nu_{23}$, and $\nu_{29}$, respectively. Likewise, a 771-$cm^{-1}$ band[19] is a likely candidate for $\nu_{26}$(ring shearing). The qualitative descriptions of the 1160- and 1100-$cm^{-1}$ bands of VLBH as a CH/CD in-plane bend and a $CH_2$ twist, respectively, were reversed upon perusal of the predicted TEDs. The IR band at 1041 $cm^{-1}$ is incorrectly attributed by VLBH to asymmetric CD out-of-plane bending, the Raman band at 726 $cm^{-1}$ being the appropriate choice. Similarly, the association of $\nu_{24}$, $\nu_{22}$, and $\nu_{25}$ at 825, 875, and 802 $cm^{-1}$, respectively, with a $CD_2$ rock and two ring modes appears questionable, and appropriate reassignments are given in Table VII. Other reinterpretations shown therein are less significant.

The vibrational assignments detailed in Table VIII for cyclopentene-$d_8$ are less complete than those for the other isotopomers. Fifteen of the bands reported by VLBH were included in the initial SQM fit, and a total of twenty of their assignments were retained after the final SQM analysis. In addition, the Raman bands at 930 and 790 $cm^{-1}$ and the IR absorptions at 849 and 724 $cm^{-1}$ were confirmed to correspond to fundamental vibrations of cyclopentene-$d_8$ but were reinterpreted as $\nu_{26}$($\beta$-$CD_2$ twist), $\nu_{13}$(CD in-plane bend), $\nu_{12}$($\alpha$-$CD_2$ twist), and $\nu_{14}$($\alpha$-$CD_2$ wag), respectively. With regard to the nine remaining fundamentals, the $\nu_{22}$(C–C stretch), $\nu_{23}$(C–C stretch), and $\nu_{32}$($\alpha$-$CD_2$ rock) modes were left unassigned because no observed gas-phase frequencies sufficiently matched the SQM predictions; yet six bands extracted from Villarreal's thesis seemed to provide reasonable assignments for $\nu_{25}$, $\nu_{10}$, $\nu_{27}$, $\nu_{28}$, $\nu_{30}$, and $\nu_{15}$. Of the latter six frequencies, the bands at 887, 764, and 716 $cm^{-1}$ were categorized as uncertain after comparison of the predicted and observed Raman intensity data. The 962-$cm^{-1}$ assignment[19] for $\nu_{10}$ is also uncertain due to the presence of a viable alternative at 950 $cm^{-1}$.[16] The Raman band reported by VLBH at 1158 $cm^{-1}$ and attributed to the asymmetric CD in-plane bend has no nearby SQM counterpart and thus is not retained as a fundamental frequency; the very weak IR band[16] at 1024 $cm^{-1}$ was omitted for similar reasons. Note that the TED analysis predicts the asymmetric CD in-plane bend to be distributed among several modes, $\nu_{22}$ at 1237 $cm^{-1}$ and $\nu_{25}$ at 1003 $cm^{-1}$ in particular. In the 840–890-$cm^{-1}$ region, VLBH assigned five distinct fundamental vibrations, but in the SQM spectrum only three are present. The intense Raman band at 878 $cm^{-1}$ was previously attributed to both an $\alpha$-$CD_2$ twist and a ring mode, whereas IR absorptions near 850 $cm^{-1}$ were assigned jointly to an in-plane CD bend and an $\alpha$-$CD_2$ rock.[16] Another IR feature at 868 $cm^{-1}$ was ascribed by VLBH to the $\beta$-$CD_2$ wag. As mentioned above, the predicted Raman intensity of $\nu_{11}$ relative to $\nu_{12}$ is selectively increased upon scaling, thus clarifying the association of $\nu_{11}$(C–C stretch) with the 878-$cm^{-1}$ band and the assignment of $\nu_{12}$($\alpha$-$CD_2$ twist) to the strong, type-C infrared absorption at 849 $cm^{-1}$. As suggested by the SQM analysis, a third band[19] at 887 $cm^{-1}$ is now tentatively assigned to $\nu_{27}$($\alpha$-$CD_2$ twist), but no other fundamental vibrations are responsible for the spectral features observed by VLBH in the 840–890-$cm^{-1}$ region.

## Summary

The cyclopentene molecule constitutes a prototype for vibrational spectroscopy of small ring compounds in the gas phase. In this work improvements have been developed in the scaled quantum mechanical (SQM) force field algorithm of Pulay and co-workers,[46] and a definitive vibrational analysis of four isotopomers of cyclopentene has been advanced. Over one hundred experimental fundamental vibrations were reproduced to within 1%, and numerous assignments have been proposed in regions where a dearth of information existed previously. The results reported here provide scale factors for use with the DZ(d) basis set and presage future applications of the SQM procedure to molecules such as $C_{60}$. In response to a challenge appearing in a paper by Laane and co-workers,[37] ab initio results of a quality which was prohibitive computationally only a few years ago have been obtained for the ring-puckering inversion barrier of cyclopentene. The final proposal of 235 ± 20 $cm^{-1}$ for the vibrationless inversion barrier is over twice as large as previous theoretical predictions but in accord with empirically determined values. For the first time a probe of zero-point vibrational effects on the effective inversion barrier of cyclopentene has been carried out with the aid of SQM vibrational data for both the planar and puckered conformations. The predicted ZPVE contribution of 20–30 $cm^{-1}$ represents a sizeable fraction of the empirically derived barrier for cyclopentene. It is hoped that the ab initio predictions reported here will stimulate further experimental investigation of this prototypical molecule.

**Acknowledgment.** The authors wish to thank Profs. P. Pulay and G. Pongor for generously providing a copy of their SCALE2 program along with the accompanying program description, thus allowing us to test the SQM subroutines in INTDER. Prof. J. Laane is also thanked for providing us a copy of J. R. Villarreal's thesis, which contained many useful details of the experimental results on which the SQM analysis was based. The research at Stanford was supported by a generous grant from Failure Analysis Associates, Inc. of San Francisco, CA, as part of a joint molecular modeling project. The provision of additional computer time by the Stanford Data Center is also acknowledged.

**Registry No.** Cyclopentene, 142-29-0; cyclopentene-*1*-*d*, 37729-44-5; cyclopentene-*1,2,3,3*-$d_4$, 59572-02-0; cyclopentene-$d_8$, 6611-46-7.

**Supplementary Material Available:** Listings of total energies at numerous levels of theory for planar ($C_{2v}$) and puckered ($C_s$) cyclopentene (Table X), the SQM quadratic force constant matrix for planar cyclopentene (Table XI), puckered → planar vibrational frequency shifts for the four isotopomers involved in the SQM analysis (Table XII), TZ(d,p) MP2 structural parameters for planar and puckered cyclopentene (Table XIII), third derivative expressions for the SQM optimization algorithm, and an extensive list of published applications of the SQM method (18 pages). Ordering information is given on any current masthead page.